

# Quantitative Study of Fluctuation Effects by Fast Lattice Monte Carlo Simulations. III. Homopolymer Brushes in an Explicit Solvent

Pengfei Zhang<sup>1,2</sup>, Baohui Li<sup>1</sup>, and Qiang Wang<sup>2\*</sup>

<sup>1</sup>School of Physics, Nankai University  
Tianjin, P. R. China 300071

<sup>2</sup>Department of Chemical and Biological Engineering  
Colorado State University  
Fort Collins, CO 80523-1370

December 20, 2011

## Abstract

Using fast lattice Monte Carlo (FLMC) simulations both in a canonical ensemble and with Wang-Landau-Transition-Matrix sampling, we have studied a model system of laterally homogeneous homopolymer brushes in an explicit solvent. Direct comparisons of the simulation results with those from the corresponding lattice self-consistent field (LSCF) theory, both of which are based on the *same* Hamiltonian (thus without any parameter-fitting between them), unambiguously and quantitatively reveal the fluctuations and correlations in the system. We have examined in detail how the Flory-Huggins interaction parameter  $\chi$  between polymer segments and solvent molecules and the number of grafted chains  $n$  affect both the brush structures and thermodynamics. For our model system, the LSCF theory is exact in the limit of  $\chi \rightarrow -\infty$ , except that it neglects the correlations among solvent

---

\*E-mail: q.wang@colostate.edu.

molecules caused by the incompressibility constraint (thus overestimating the solvent entropy). At finite  $n$  and  $\chi$ , the segmental density profile in the direction perpendicular to the grafting substrate obtained from FLMC simulations is flatter than the LSCF prediction, and the free-end density from FLMC simulations is also lower than the LSCF prediction close to the substrate. At finite  $n$  and  $\chi > 0$ , the LSCF theory overestimates the internal energy. In addition, it underestimates the difference in free energy but overestimates that in entropy from the reference state in the limit of  $\chi \rightarrow -\infty$  at small  $\chi \geq 0$ , and the opposite occurs at larger  $\chi$ . At large  $n$ , FLMC results approach LSCF predictions at a rate of  $1/n$  in most cases.

# 1 Introduction

This is the third paper in our series of study,<sup>1,2</sup> where fast lattice Monte Carlo (FLMC) simulations<sup>3</sup> are directly compared with the corresponding lattice polymer field theories based on the same model system (Hamiltonian), thus without any parameter-fitting, to unambiguously and quantitatively reveal the effects of fluctuations and correlations either neglected or treated approximately in the theories. In the second paper in this series (referred to as Paper II hereafter), we studied monodisperse, uncharged and flexible homopolymer brushes on a planar and nonadsorbing substrate in an implicit, good solvent.<sup>2</sup> Here we extend that study to the case of an explicit solvent.

As explained in Paper II, in the most widely used self-consistent field (SCF) theory,<sup>4</sup> an implicit solvent is described by the second virial coefficient  $v$  (with the third virial coefficient  $w$  also needed for a poor solvent), and an explicit solvent is described by the Flory-Huggins  $\chi$  parameter for the interactions between polymer segments and solvent molecules along with the incompressibility constraint requiring the total volume fraction of polymer and solvent be 1 everywhere, which includes all the higher-order terms neglected in the theoretical treatment of an implicit solvent. As shown below, the incompressibility constraint may limit the allowed chain conformations in a brush, which makes such cases more difficult to analyze. It also leads to correlations among solvent molecules; SCF theory neglects such correlations, thus overestimating the entropy of solvent molecules. We refer readers to the Introduction of Paper II for an overview of some previous SCF studies on the brushes in an explicit solvent.<sup>5–22</sup>

The meaning of implicit/explicit solvent is somewhat different in molecular simulations. The vacancies (unoccupied lattice sites) in conventional lattice Monte Carlo (MC) simulations of the brushes<sup>9,23–31</sup> can be considered as an explicit solvent due to the self- and mutual-avoiding walk (i.e., the incompressibility constraint) used. On the other hand, in off-lattice simulations of the brushes,<sup>32–44</sup> an explicit (or implicit) solvent simply means that solvent molecules are explicitly (or not) included in the system; in such simulations, the above incompressibility constraint clearly cannot be enforced and  $v$  (and  $w$ ) is rarely used (except in Refs. [43,44]).

As explained in detail in the Introduction of Paper II, while various forms of SCF theory have been compared with molecular simulations<sup>9,23,25,26,31–33,35–37,43,45</sup> (for example, Pépin and Whitmore compared their lattice MC simulations with continuum SCF calculations both in an explicit and good solvent<sup>9</sup>), which provided important insights and greatly furthered our understanding of polymer brushes, none of these comparisons

was done using exactly the same model system in both SCF theories and molecular simulations. They therefore could not unambiguously distinguish the model differences from the consequences of the mean-field approximation inherent in all SCF theories. In addition, only structures (e.g., segmental distributions, brush height, and bond orientation) but not thermodynamics (e.g., internal energy, free energy, and entropy) of the brushes have been examined. This motivated our study presented in Paper II and here, which are the prerequisite for developing more accurate theories for polymer brushes.

One complication for the brushes in a poor solvent is the possible formation of laterally inhomogeneous structures, which requires both FLMC simulations and LSCF calculations be performed in 3D. The Wang-Landau-Transition-Matrix sampling<sup>46–48</sup> we use to study the brush thermodynamics, however, is computationally very expensive for multi-chain systems in 3D due to the large number of micro/macrostates. We therefore limit this work to laterally homogeneous brushes in 1D, which is justified by the lateral instability analysis as shown in Sec. 3 below, and report our 3D study of phase transitions of grafted chains in an explicit, poor solvent in another paper.<sup>49</sup> Our 2D and 3D canonical-ensemble FLMC simulations of the brushes in an implicit, good solvent reported in Paper II further indicate that, while the differences between FLMC and LSCF results caused solely by the system fluctuations/correlations are smaller in higher dimensions, most qualitative features can be studied in 1D.

## 2 Model and Methods

### 2.1 Model system

We consider an incompressible polymer brush system consisting of  $n$  chains of homopolymer A each having  $N$  segments and  $n_S$  solvent molecules on a lattice having  $L = N$  lattice layers in the  $x$  direction; for the 1D lattice, the total number of lattice sites  $V = L$ . Each homopolymer segment or solvent molecule occupies one lattice site, and each lattice site is occupied by totally  $\rho_0 \equiv (nN + n_S) / V$  segments and solvent molecules. The first segment of all chains is grafted at  $x = 1$  (i.e., in the first layer), and an impenetrable wall is placed at  $x = 0$ , which cannot be occupied by either polymer segments or solvent molecules. The canonical-ensemble partition function is

$$\mathcal{Z} = \frac{1}{n!n_S!} \prod_{k=1}^n \prod_{s=1}^N \sum_{X_{k,s}} \cdot \prod_{k=1}^{n_S} \sum_{x_k} \cdot \exp \left\{ -\beta \sum_{k=1}^n h_k^C - \beta \mathcal{H}^E \right\} \cdot \prod_x \delta_{\hat{\rho}(x) + \hat{\rho}_S(x), \rho_0} \quad (1)$$

where  $X_{k,s}$  denote the spatial position of the  $s^{\text{th}}$  segment on the  $k^{\text{th}}$  chain,  $x_k$  denotes the position of the  $k^{\text{th}}$  solvent molecule, the summations are over all possible positions of all polymer segments and solvent molecules, respectively, “.” means that the products before it do not apply to the terms after it but the summations before it do, and  $\beta \equiv 1/k_B T$  with  $k_B$  being the Boltzmann constant and  $T$  the absolute temperature.  $h_k^C$  is the Hamiltonian of the  $k^{\text{th}}$  chain due to its chain connectivity;  $\beta h_k^C = 0$  if the chain connectivity is maintained and  $\infty$  otherwise. Finally, the Hamiltonian due to non-bonded interactions is given by

$$\beta \mathcal{H}^E [\hat{\rho}, \hat{\rho}_S] = \frac{\chi}{\rho_0} \sum_x [\hat{\rho}(x) \hat{\rho}_S(x) - n(\rho_0 - n)] \quad (2)$$

where  $\chi$  is the Flory-Huggins parameter characterizing the interaction between polymer segments and solvent molecules, the microscopic number density of polymer segments and solvent molecules at lattice site  $x$  is given by  $\hat{\rho}(x) \equiv \sum_{k=1}^n \sum_{s=1}^N \delta_{x, X_{k,s}}$  and  $\hat{\rho}_S(x) \equiv \sum_{k=1}^{n_S} \delta_{x, x_k}$ , respectively, and  $\delta_{x, X_{k,s}}$  denotes the Kronecker  $\delta$ -function. The last term in Eq. (2) is included such that  $\beta \mathcal{H}^E = 0$  for a *homogeneous* system.

With the incompressibility constraint imposed by the last term in Eq. (1), we can re-write  $\beta \mathcal{H}^E[\hat{\rho}] = -C\chi NE/\rho_0^2$ , where  $C \equiv n/\bar{\phi}V$  with the average polymer volume fraction  $\bar{\phi} \equiv nN/(nN + n_S)$ ,  $E[\hat{\rho}] \equiv \sum_x [\hat{\rho}(x) - \bar{\phi}\rho_0]^2$  is defined as the energy level of our system, and we have used  $V = N$ . The partition function in Eq. (1) can then be re-written as

$$\mathcal{Z} = \frac{1}{n!n_S!} \prod_{k=1}^n \prod_{s=1}^N \sum_{X_{k,s}} \cdot \frac{n_S!}{\prod_x [\rho_0 - \hat{\rho}(x)]!} \exp \left\{ -\beta \sum_{k=1}^n h_k^C + C\chi N \frac{E}{\rho_0^2} \right\} \cdot \prod_x \theta(\rho_0 - \hat{\rho}(x)) \quad (3)$$

where  $\theta(x) = 1$  if  $x \geq 0$  and 0 otherwise. Here we have eliminated the dependence on the spatial positions of all solvent molecules  $\{x_k\}$  in the summation, and  $\frac{n_S!}{\prod_x [\rho_0 - \hat{\rho}(x)]!}$  is the number of different ways of arranging these solvent molecules for a given configuration  $\{X_{k,s}\}$  of all chains. In Appendix A, we give an approximate correspondence between this model system for brushes in an explicit solvent and that for brushes in an implicit solvent studied in Paper II.<sup>2</sup>

## 2.2 Fast lattice Monte Carlo simulations

### 2.2.1 Canonical-ensemble simulations

Some of our FLMC simulations are performed in a canonical ensemble, where  $n$ ,  $V = L = N$ ,  $n_S$  and  $\chi$  are fixed. We use the same configurationally biased trial moves as in Paper II.

To take into account the entropy of solvent molecules, however, the Rosenbluth weight<sup>50</sup>  $R$  used in the acceptance criterion in Paper II must be multiplied by  $W \equiv \prod_x [\rho_0 - \hat{\rho}(x)]!$  for the corresponding configuration, i.e.,  $R \rightarrow WR$  for both the trial and old configurations. About  $4 \sim 20 \times 10^6$  Monte Carlo steps (MCS) are performed in each simulation, where one MCS is defined as  $nN$  trial moves. The error bar of each ensemble-averaged quantity is estimated in the same way as in the first paper<sup>1</sup> in our series (referred to as Paper I hereafter).

### 2.2.2 Wang-Landau–Transition-Matrix (WL-TM) sampling

As in Papers I and II, we use the combined WL-TM sampling<sup>46–48</sup> to estimate the density of states (DoS) within a chosen  $E$ -range. The partition function in Eq. (3) can be rewritten as

$$\mathcal{Z} = \sum_E \Omega(E) \exp\left(C\chi N \frac{E}{\rho_0^2}\right) \quad (4)$$

with DoS  $\Omega(E)$  defined as

$$\Omega(E) \equiv \frac{1}{n!} \prod_{k=1}^n \prod_{s=1}^N \sum_{X_{k,s}} \frac{\delta_{E,E[\hat{\rho}]}}{\prod_x [\rho_0 - \hat{\rho}(x)]!} \exp\left\{-\beta \sum_{k=1}^n h_k^C\right\} \cdot \prod_x \theta(\rho_0 - \hat{\rho}(x)) \quad (5)$$

Note that  $\Omega(E) = 0$  for odd  $E$  in our simulations, and such macrostates are not included here. We use the same trial moves as in our canonical-ensemble simulations, and the details of our WL-TM sampling are given in Paper II. As explained above, however,  $R$  used in Paper II now needs to be replaced by  $WR$  for both the trial and old configurations.

Note that the normalized DoS  $g(E)$  obtained from WL-TM simulations gives  $g(E=0) = 1$ . Since DoS of the ground state of our  $n$ -chain system (where all chains are fully stretched) is  $\Omega(E=0) = 1/n! [(\rho_0 - n)!]^V$ , we have  $\Omega(E) = g(E)/n! [(\rho_0 - n)!]^V$  (for conciseness, the explicit dependence of  $\Omega(E)$  and  $g(E)$  on  $n$  is omitted in our notation).

Once  $g(E)$  is obtained, we can compute the Helmholtz free energy per chain of length  $N$  (i.e., per  $N$  lattice sites)

$$\beta f_{c,\text{FLMC}}(\chi) \equiv -N \frac{\ln \mathcal{Z}(\chi)}{\rho_0 V} = -\frac{\bar{\phi}}{n} \ln \sum_E \frac{g(E)}{n! [(\rho_0 - n)!]^V} \exp\left(C\chi N \frac{E}{\rho_0^2}\right) \quad (6)$$

and any canonical-ensemble average as a function of  $\chi$ . For the latter, we define the normalized probability distribution of  $E$  at given  $\chi$  as

$$P(E, \chi) = \frac{g(E)}{n! [(\rho_0 - n)!]^V} \exp\left(C\chi N \frac{E}{\rho_0^2}\right) / \mathcal{Z}(\chi) \quad (7)$$

The internal energy per chain is then

$$\beta u_{c,\text{FLMC}}(\chi) \equiv N \frac{\langle \beta \mathcal{H}^E(\chi) \rangle}{\rho_0 V} = -\frac{\chi N}{V} \frac{\langle E(\chi) \rangle}{\rho_0^2} = -\frac{\chi N}{V} \sum_E \frac{E}{\rho_0^2} P(E, \chi) \quad (8)$$

and the entropy per chain can be obtained from the thermodynamic relation

$$s_c(\chi)/k_B = \beta u_c(\chi) - \beta f_c(\chi) \quad (9)$$

The specific heat per chain is

$$C_{v,\text{FLMC}}(\chi)/k_B \equiv \frac{N}{\rho_0 V} \left[ \langle \beta \mathcal{H}^E(\chi)^2 \rangle - \langle \beta \mathcal{H}^E(\chi) \rangle^2 \right] = \frac{C(\chi N)^2}{V \rho_0^4} \left[ \langle E(\chi)^2 \rangle - \langle E(\chi) \rangle^2 \right] \quad (10)$$

Finally, the canonical-ensemble averages of the mean-square chain end-to-end distance  $R_{e,\text{FLMC}}^2(\chi)$ , the mean-square chain radius of gyration  $R_{g,\text{FLMC}}^2(\chi)$  and the brush height  $h_{\text{FLMC}}(\chi)$  are calculated in the same way as in Paper II, except that the parameter  $N/\kappa$  there is replaced by  $\chi$ .

### 2.2.3 Enumeration

One advantage of working in 1D is that we can use enumeration to obtain the exact DoS  $\Omega_{\text{exact}}(E)$  for the single-chain system; all of our FLMC results shown for  $n = 1$  are actually obtained from enumeration and thus exact. These are further used in our error estimation as discussed in detail later.

## 2.3 Lattice self-consistent field theory

Here we start with the *same* Hamiltonian as in our FLMC simulations, and insert in Eq. (1) the identity  $1 = (\rho_0/2\pi)^{2L} \int d\phi d\omega d\phi_S d\omega_S \exp[i\omega \cdot (\rho_0 \phi - \hat{\rho})] \exp[i\omega_S \cdot (\rho_0 \phi_S - \hat{\rho}_S)]$ , where vectors  $\hat{\rho} \equiv \{\hat{\rho}(x)\}$  and  $\hat{\rho}_S \equiv \{\hat{\rho}_S(x)\}$  have  $L$  elements,  $\phi \equiv \{\phi(x)\}$  and  $\phi_S \equiv \{\phi_S(x)\}$  are the normalized density (volume fraction) fields of polymer segments and solvent molecules, respectively, constrained to  $\hat{\rho}/\rho_0$  and  $\hat{\rho}_S/\rho_0$ , and  $\omega \equiv \{\omega(x)\}$  and

$\omega_S \equiv \{\omega_S(x)\}$  are the conjugate fields imposing these constraints, respectively. We then substitute the following integral form of the  $\delta$ -function into Eq. (1),

$$\prod_x \delta_{\hat{\rho}(x)+\hat{\rho}_S(x),\rho_0} = \frac{1}{(2\pi)^L} \int d\boldsymbol{\eta} \exp[-\rho_0 i\boldsymbol{\eta} \cdot (\boldsymbol{\phi} + \boldsymbol{\phi}_S - \mathbf{1})], \quad (11)$$

where the vector  $\boldsymbol{\eta} \equiv \{\eta(x)\}$  is the conjugate field imposing the incompressibility constraint and  $\mathbf{1}$  has  $L$  elements of 1. We finally have  $\mathcal{Z} = [\rho_0^{2L}/(2\pi)^{3L}] \int d\boldsymbol{\phi} d\boldsymbol{\omega} d\boldsymbol{\phi}_S d\boldsymbol{\omega}_S d\boldsymbol{\eta} \exp\{- (n/\bar{\phi}) \beta f_c[\boldsymbol{\phi}, i\boldsymbol{\omega}, \boldsymbol{\phi}_S, i\boldsymbol{\omega}_S, i\boldsymbol{\eta}]\}$  with

$$\begin{aligned} \beta f_c = & \chi \boldsymbol{\phi} \cdot \boldsymbol{\phi}_S - \frac{1}{N} \boldsymbol{\phi} \cdot i\boldsymbol{\omega} - \frac{1}{N} \boldsymbol{\phi}_S \cdot i\boldsymbol{\omega}_S + \frac{1}{N} i\boldsymbol{\eta} \cdot (\boldsymbol{\phi} + \boldsymbol{\phi}_S - \mathbf{1}) \\ & - \chi N \bar{\phi} (1 - \bar{\phi}) - \bar{\phi} \ln Q[i\boldsymbol{\omega}] - N (1 - \bar{\phi}) \ln Q_S[i\boldsymbol{\omega}_S] + \beta f_c^{id}, \end{aligned} \quad (12)$$

where the single-chain partition function  $Q[i\boldsymbol{\omega}] \equiv \prod_{s=1}^N \sum_{X_s} \cdot \exp[-\beta h^C - i \sum_{s=1}^N \omega(X_s)/N] / G$  with  $G \equiv \prod_{s=1}^N \sum_{X_s} \cdot \exp(-\beta h^C) = z^{N-1} L$  and the lattice coordination number  $z = 2$  in our 1D case, the single-particle partition function  $Q_S[i\boldsymbol{\omega}_S] \equiv \sum_x \exp[-i\omega_S(x)/N] / L$ , the free energy per chain of length  $N$  for an ideal system of  $n$  *ungrafted* chains and  $n_S$  solvent molecules (which is non-interacting and *not* subject to the incompressibility constraint)

$$\beta f_c^{id} \equiv -\frac{\bar{\phi}}{n} \ln \frac{G^n}{n! n_S!} - N (1 - \bar{\phi}) \ln V = -\frac{s_c^{id}}{k_B} \quad (13)$$

with  $s_c^{id}$  denoting the entropy per chain for the ideal system, and we have re-scaled variables according to  $N\boldsymbol{\omega} \rightarrow \boldsymbol{\omega}$ ,  $N\boldsymbol{\omega}_S \rightarrow \boldsymbol{\omega}_S$  and  $N\boldsymbol{\eta} \rightarrow \boldsymbol{\eta}$ .

The SCF equations are obtained by setting  $\delta\beta f_c/\delta\phi(x) = \delta\beta f_c/\delta i\omega(x) = \delta\beta f_c/\delta\phi_S(x) = \delta\beta f_c/\delta i\omega_S(x) = \delta\beta f_c/\delta i\eta(x) = 0$  (i.e., the mean-field approximation<sup>4</sup>) and given by

$$i\omega(x) = \chi N \phi_S(x) + i\eta(x) \quad (14)$$

$$i\omega_S(x) = \chi N \phi(x) + i\eta(x) \quad (15)$$

$$\phi(x) = \sum_{s=1}^N \phi_s(x) \quad (16)$$

$$\phi_s(x) = \frac{\bar{\phi} \exp[i\omega(x)/N]}{q_N^*(x=1)} q_s(x) q_{N+1-s}^*(x) \quad (17)$$

$$\phi_S(x) = \frac{1 - \bar{\phi}}{Q_S[i\omega_S]} \exp\left[-\frac{i\omega_S(x)}{N}\right] \quad (18)$$

$$\phi(x) + \phi_S(x) = 1 \quad (19)$$

where  $\phi_s(x)$  is the volume fraction of the  $s^{\text{th}}$  segment of all chains at  $x$ ,  $q_s(x)$  is the probability of finding a partial chain of  $s$  segments starting from the grafted end and ending at position  $x$  in the system, and  $q_t^*(x)$  is the probability of finding a partial chain of  $t \equiv N + 1 - s$  segments starting from the free end and ending at  $x$  in the system. According to the chain connectivity, we have the recursive relations

$$q_{t+1}^*(x) = \exp\left[-\frac{i\omega(x)}{N}\right] \frac{q_t^*(x-1) + q_t^*(x+1)}{2}, \quad q_{t=1}^*(x) = \exp\left[-\frac{i\omega(x)}{N}\right] \quad (20)$$

$$q_{s+1}(x) = \exp\left[-\frac{i\omega(x)}{N}\right] \frac{q_s(x-1) + q_s(x+1)}{2}, \quad q_{s=1}(x) = \exp\left[-\frac{i\omega(x)}{N}\right] \delta_{x,1} \quad (21)$$

It is worthy to note that, if  $\{i\omega, i\omega_S, i\eta\}$  is a solution of the SCF equations,  $\{i\omega + c, i\omega_S + c, i\eta + c\}$  is also a solution with  $c$  being an arbitrary constant; the corresponding  $\{\phi, \phi_S\}$  and  $\beta f_{c,\text{LSCF}}$  remain unchanged. We therefore set  $Q_S = 1 - \bar{\phi}$  to obtain a unique solution. Then from Eqs. (14), (15), (18) and (19) we obtain

$$i\omega(x) = -N \ln[1 - \phi(x)] + \chi N [1 - 2\phi(x)] \quad (22)$$

This, along with Eq. (16), is solved using the Broyden method combined with a globally convergent strategy,<sup>51</sup> where the maximum residual error at all  $x$  is less than  $10^{-12}$ .

Once the SCF equations are solved, we calculate the free energy per chain as

$$\beta(f_{c,\text{LSCF}} - f_c^{id}) = \sum_x \{\chi\phi^2(x) + \ln[1 - \phi(x)]\} - \chi N \bar{\phi}(1 - \bar{\phi}) - \bar{\phi} \ln Q - N(1 - \bar{\phi}) \ln(1 - \bar{\phi}) \quad (23)$$

with  $Q = q_N^*(x=1)/L$  (where Eq. (22) is used), the internal energy per chain as

$$\beta u_{c,\text{LSCF}} = -\frac{\chi N}{V} \frac{E_{\text{LSCF}}}{\rho_0^2} \quad (24)$$

with

$$\frac{E_{\text{LSCF}}}{\rho_0^2} \equiv \sum_x [\phi(x) - \bar{\phi}]^2 \quad (25)$$

and the entropy per chain  $s_{c,\text{LSCF}}/k_B$  through Eq. (9). The LSCF predictions of the mean-square chain end-to-end distance  $R_{e,\text{LSCF}}^2$  and radius of gyration  $R_{g,\text{LSCF}}^2$  are calculated in the same way as in Paper II, and the brush height  $h_{\text{LSCF}} \equiv 2 \sum_{x=1}^L (x-1)\phi(x)/\bar{\phi}L$ .

It is easy to show that, for a *homogeneous* incompressible system of *ungrafted* chains and solvent molecules, our LSCF theory with Kronecker  $\delta$ -function interactions reduces to the standard Flory-Huggins theory as expected. On the other hand, Appendix A gives the correspondence between our brushes in an explicit solvent and those in an implicit solvent studied in Paper II; that is, when  $\phi(x) \ll 1$ ,  $(1 - 2\chi)N\bar{\phi}$  and  $\phi(x)/\bar{\phi}$  here correspond to  $N/\kappa$  and  $\phi(x)$  in Paper II, respectively.

### 2.3.1 LSCF predictions in the limits of $\chi \rightarrow \pm\infty$

In the limit of  $\chi \rightarrow -\infty$ , the system is in the ground state with no fluctuations, where all chains are fully stretched with no correlations among them, and the LSCF predictions of  $\phi(x) = \bar{\phi}$  for  $x \in [1, N]$ ,  $\phi_{s=N}(x) = 1$  at  $x = N$  (and 0 otherwise),  $E = \beta u_c = 0$ ,  $R_e^2 = (N-1)^2$ ,  $R_g^2 = (N^2-1)/12$ , and  $h = N-1$  are exact. LSCF theory further gives  $GQ = 1$  in this limit, thus  $\beta(f_{c,\text{LSCF}} - f_c^{\text{id}}) = -(s_{c,\text{LSCF}} - s_c^{\text{id}})/k_B = \bar{\phi} \ln G$ ;<sup>52</sup> the latter, however, is not exact for any finite  $n_S$ -value due to the correlations among solvent molecules caused by the incompressibility constraint.

To understand this, let us consider  $s_c$  in the general case where  $n_S$  solvent molecules are arranged for a given  $\{\phi(x)\}$  according to the incompressibility constraint. The exact microcanonical-ensemble partition function for the solvent is  $\Omega^S = 1/\prod_{x=1}^L [\rho_0 \phi_S(x)]!$  with  $\phi_S(x) \equiv 1 - \phi(x)$ , leading to the exact solvent entropy per chain

$$\frac{s_{c,\text{exact}}^S}{k_B} \equiv \frac{N \ln \Omega^S}{\rho_0 V} = -\frac{N}{\rho_0 V} \sum_x \ln[\rho_0 \phi_S(x)]! \quad (26)$$

LSCF theory, however, neglects the correlations among solvent molecules caused by the incompressibility constraint and gives<sup>52</sup>

$$\frac{s_{c,\text{LSCF}}^S}{k_B} = \frac{1}{\rho_0} \ln \frac{V^{n_S}}{n_S!} + N(1 - \bar{\phi}) \ln(1 - \bar{\phi}) - \sum_x \phi_S(x) \ln \phi_S(x) \quad (27)$$

Using the Stirling approximation, it is easy to show that  $s_{c,\text{exact}}^S - s_{c,\text{LSCF}}^S \rightarrow 0$  as  $n_S \rightarrow \infty$  (i.e.,  $\rho_0 \rightarrow \infty$  at constant  $\bar{\phi}$ ).

In the limit of  $\chi \rightarrow \infty$ , the system is in the “ceiling” state with the largest  $E/\rho_0^2$ , and it is clear that  $\beta u_c \rightarrow -\infty$  and thus  $\beta f_c \rightarrow -\infty$  for  $N \geq 3$ . Two cases need to be considered separately:

(1) When  $\bar{\phi} \leq \lfloor \frac{N+1}{2} \rfloor^{-1}$  (where  $\lfloor a \rfloor$  denotes the integer part of a non-negative number  $a$ ), the incompressibility constraint does not limit chain conformations. In the limit of  $\chi \rightarrow \infty$ , all chains are fully collapsed (i.e.,  $X_s = 1$  for odd  $s$  and 2 for even  $s$ ), and LSCF theory gives  $GQ = 1$ , which corresponds to the total number of chain conformations of a single grafted chain.<sup>52</sup> For odd  $N$ , LSCF theory gives the following exact results:  $\phi(x) = \frac{N+1}{2}\bar{\phi}$  at  $x = 1$ ,  $\frac{N-1}{2}\bar{\phi}$  at  $x = 2$ , and 0 otherwise;  $\phi_{s=N}(x) = 1$  at  $x = 1$ , and 0 otherwise;  $E/\rho_0^2 = \frac{(N-1)^2}{2}\bar{\phi}^2$ ;  $h = 1 - \frac{1}{N}$ ,  $R_e^2 = 0$ , and  $R_g^2 = \frac{1}{4} - \frac{1}{4N^2}$ . As shown above, its prediction<sup>52</sup> of  $(s_{c,\text{LSCF}} - s_c^{\text{id}})/k_B = -\bar{\phi} \ln G - (1 - \frac{N+1}{2}\bar{\phi}) \ln(1 - \frac{N+1}{2}\bar{\phi}) - (1 - \frac{N-1}{2}\bar{\phi}) \ln(1 - \frac{N-1}{2}\bar{\phi}) + N(1 - \bar{\phi}) \ln(1 - \bar{\phi})$  is not exact for any finite  $n_S$ -value due to the correlations among solvent molecules. For even  $N$ , LSCF theory gives the following exact results:  $\phi(x) = \frac{N}{2}\bar{\phi}$  at  $x = 1$  and 2, and 0 otherwise;  $\phi_{s=N}(x) = 1$  at  $x = 2$ , and 0 otherwise;  $E/\rho_0^2 = \frac{N^2-2N}{2}\bar{\phi}^2$ ;  $h = 1$ ,  $R_e^2 = 1$ , and  $R_g^2 = \frac{1}{4}$ . Its prediction<sup>52</sup> of  $(s_{c,\text{LSCF}} - s_c^{\text{id}})/k_B = -\bar{\phi} \ln G - 2(1 - \frac{N}{2}\bar{\phi}) \ln(1 - \frac{N}{2}\bar{\phi}) + N(1 - \bar{\phi}) \ln(1 - \bar{\phi})$  is again not exact for any finite  $n_S$ -value.

(2) When  $\bar{\phi} > \lfloor \frac{N+1}{2} \rfloor^{-1}$ , the incompressibility constraint limits chain conformations. In the limit of  $\chi \rightarrow \infty$ , chains are therefore in the most collapsed states as permitted by the incompressibility. The “ceiling” state is in general degenerated (i.e.,  $GQ > 1$ <sup>52</sup>) with  $E/\rho_0^2 = -A\bar{\phi}(1 - A\bar{\phi}) - B\bar{\phi}(1 - B\bar{\phi}) + N\bar{\phi}(1 - \bar{\phi})$ , where  $A = \lfloor \frac{N}{2} - \lfloor \frac{N}{2}\bar{\phi} \rfloor / \bar{\phi} \rfloor$  and  $B = N - 2\lfloor \frac{N}{2}\bar{\phi} \rfloor / \bar{\phi} - A$ . These values of A and B can be found in the following way: Let us first consider the single-chain system. One of the allowed chain conformations in the most collapsed state gives  $\phi(x) = 1$  for  $x \leq x_0 \equiv 2\lfloor \frac{N}{2}\bar{\phi} \rfloor$ ,  $< 1$  at  $x_1 \equiv x_0 + 1$  and  $x_2 \equiv x_0 + 2$ , and 0 otherwise. That is, there are totally  $2\lfloor \frac{N}{2}\bar{\phi} \rfloor \rho_0 = 2\lfloor \frac{N}{2}\bar{\phi} \rfloor / \bar{\phi}$  segments at lattice sites  $1 \leq x \leq x_0$ ,  $\lfloor (N - 2\lfloor \frac{N}{2}\bar{\phi} \rfloor / \bar{\phi}) / 2 \rfloor = A$  segments at  $x_2$ , and  $B$  segments at  $x_1$ . For multi-chain systems, this chain conformation can be applied to all the chains, leading to the above  $E/\rho_0^2$  which is independent of  $n$ . This exact result is therefore also the LSCF prediction (i.e., in the limit of  $n \rightarrow \infty$ ). When  $\frac{N}{2}\bar{\phi}$  is an integer, LSCF theory gives the exact result of  $\phi(x) = 1$  for  $x \in [1, N\bar{\phi}]$  and 0 otherwise, thus the exact result of  $h = N\bar{\phi} - 1$ ;  $\phi_{s=N}(x)$ , however, depends on  $n$  and its exact result therefore cannot be predicted by LSCF theory, so are  $R_e^2$  and  $R_g^2$ . When  $N\bar{\phi}/2$  is not an integer, the exact results of  $\phi(x)$  and  $\phi_{s=N}(x)$  cannot be predicted by LSCF theory, so are  $h$ ,  $R_e^2$  and  $R_g^2$ . Finally, since  $GQ$  is in general not known analytically,<sup>52</sup> we do not have an expression for  $s_{c,\text{LSCF}}$ , which cannot be exact for any finite  $n_S$ -value as explained above.

From the above analysis, it is clear that the limit of  $\chi \rightarrow -\infty$  provides a well understood reference state, which is used in the following.

### 3 Results and Discussion

Our model system of brushes in an explicit solvent is specified by a few physical parameters: the chain length  $N$ , the average polymer volume fraction  $\bar{\phi} = n/\rho_0$ , the Flory-Huggins interaction parameter  $\chi$  between polymer segments and solvent molecules, and the number of grafted chains  $n$ ; the first three completely determine the LSCF results, and the last one controls system fluctuations in FLMC simulations, which approach LSCF predictions in the limit of  $n \rightarrow \infty$ . Different from the compressible polymer melts studied in Paper I or the brushes in an implicit solvent studied in Paper II, here  $N$  characterizes both the chain discretization and the polymer/solvent size ratio; it is therefore a physical parameter instead of a model parameter. Unless specified otherwise, our results presented here are for  $N = 40$  and  $\bar{\phi} = 0.1$ ; similar results are found for other values of  $N$  and  $\bar{\phi}$ .

In this 1D study, we are mainly interested in the range of  $0 \leq \chi \leq 1.5$ ; both LSCF calculations and FLMC simulations at much larger  $\chi$ -values are found to be challenging. To justify our 1D study of brushes in a poor solvent, we have analyzed the lateral instability of our LSCF results obtained under the assumption of lateral homogeneity, following Refs. [53, 54]; our approach is similar to that in Ref. [54], except that we use lattice polymers (instead of continuous Gaussian chains) and equal bulk number density for polymer segments and solvent molecules. For  $N = 40$  and  $\bar{\phi} = 0.1$ , the laterally homogeneous brush is found to be stable for  $\chi < 1.575$  on any 2D and 3D lattices having  $z_0 = 0$  as the 1D lattice (thus the same LSCF results for the laterally homogeneous brush), where  $z_0$  denotes the fraction of the nearest-neighbor lattice sites that are at the same  $x$  of a given lattice site; one example of such 3D lattice is the body-centered cubic lattice. Finally, to show the bridging to our reference system in the limit of  $\chi \rightarrow -\infty$ , some of our results are presented as a function of  $\chi/(3 - \chi)$  in the range of  $[-1, 1]$ .

#### 3.1 Density of states and error estimation

Fig. 1(a) shows  $g(E)$  obtained from our WL-TM simulations for systems of various  $n \geq 2$ ; the exact  $g(E)$  obtained from enumeration for  $n = 1$  is also shown. We see that  $g(E)$  increases with increasing  $E$  at small  $E$  and decreases at large  $E$ , and that  $g(E)$  oscillates

slightly at large  $E$  due to the use of a lattice. In addition, the  $E$ -range is broader for systems with larger  $n$ , as expected. The normalized probability distribution  $P(E, \chi)$  is shown in Fig. 1(b) for systems with  $n = 1$  and 16 at  $\chi = 0$  and  $\chi = 1.5$ . We see that  $E$  of those states contributing significantly to canonical-ensemble averages increases with increasing  $\chi$  and  $n$ , and that the  $E$ -ranges we choose are broad enough for computing canonical-ensemble averages in the range of  $\chi$  from  $-\infty$  to 1.5.

Following Paper I, for the single-chain system we define the error in  $\ln g(E)$  per macrostate as  $\epsilon \equiv \sqrt{\sum_E [\ln g(E) - \ln g_{\text{exact}}(E)]^2 / N_E}$ , where  $N_E$  denotes the total number of even  $E$ -macrostates contained in the  $E$ -window, and the (related) error in  $\beta f_{c,\text{FLMC}}(\chi)$  as

$$\begin{aligned} \epsilon_f(\chi) &\equiv |\beta f_{c,\text{FLMC}} - \beta f_{c,\text{exact}}| \\ &= \frac{\bar{\phi}}{n} \left| \ln \sum_E g(E) \exp\left(C\chi N \frac{E}{\rho_0^2}\right) - \ln \sum_E g_{\text{exact}}(E) \exp\left(C\chi N \frac{E}{\rho_0^2}\right) \right| \end{aligned} \quad (28)$$

where  $g(E)$  is obtained from WL-TM simulations and  $g_{\text{exact}}(E) \equiv \Omega_{\text{exact}}(E)/\Omega_{\text{exact}}(E=0)$  obtained by enumeration. Fig. 2(a) shows that  $\epsilon$  and  $\epsilon_f$  (at  $\chi = 0, 1$  and 1.5) decrease gradually with increasing number of MCS in TM simulations (TM MCS), and that  $\epsilon_f < 0.006$  in our single-chain simulation at  $4 \times 10^7$  TM MCS. Fig. 2(b) shows  $\beta f_{c,\text{FLMC}} - \beta f_{c,\text{exact}}$  as a function of  $\chi$  at  $4 \times 10^7$  TM MCS for the single-chain systems with  $N = 20$  and 40; note that Eq. (28) gives  $\epsilon_f(\chi \rightarrow -\infty) = 0$ . While  $\epsilon_f(\chi)$  exhibits a maximum as  $\chi$  varies in both cases, its location is outside the  $\chi$ -range that we are interested in. At large  $\chi$ ,  $\beta f_{c,\text{FLMC}} - \beta f_{c,\text{exact}}$  approaches a constant, the value of which is mainly determined by the error of our  $g(E)$  for the ‘‘ceiling’’ state (i.e.,  $E = 180$  for  $N = 20$  and 360 for  $N = 40$ ).

Different from the brushes in an implicit solvent studied in Paper II (i.e, the application of Eq. (28) there), there is no *finite*  $\chi$ -value at which chains are uncorrelated for the brushes in an explicit solvent (even at  $\chi = 0.5$ , where only the second virial coefficient vanishes). To estimate the error in  $\beta f_c$  for our multi-chain systems with  $n \geq 2$ , where  $g_{\text{exact}}(E)$  is not known, we follow Paper I and plot in Figs. 2(c) and 2(d)  $\beta f_{c,\text{FLMC}}$  as a function of the number of TM MCS for systems with  $n = 2$  and 16 at  $\chi = 0$  and 1.5. We see that in all the cases  $\beta f_{c,\text{FLMC}}$  increases towards an asymptotic value with increasing number of TM MCS, and that  $4 \times 10^7$  TM MCS give an error in  $\beta f_{c,\text{FLMC}}$  (difference from the value at  $2 \times 10^7$  TM MCS) of less than 0.003 and 0.00012 at  $\chi = 0$  for  $n = 2$  and 16, respectively, and less than 0.002 and 0.00003 at  $\chi = 1.5$  for  $n = 2$  and 16, respectively. As found in Paper I, the error in  $\beta f_{c,\text{FLMC}}$  from our WL-TM simulations decreases with increasing  $n$ . Hereafter we use the simulation results at  $4 \times 10^7$  TM MCS for  $n \geq 2$ .

## 3.2 Brush structures

### 3.2.1 Segmental density profile and brush height

Fig. 3(a) shows  $\phi(x)$  obtained from canonical-ensemble simulations (denoted by  $\phi_{\text{FLMC}}(x)$ ) with various  $n$  at  $\chi = 1$ , along with the corresponding LSCF predictions (denoted by  $\phi_{\text{LSCF}}(x)$ ). In such a poor solvent, polymer segments collapse near the substrate. As found in Paper II,  $\phi_{\text{FLMC}}(x)$  is flatter than  $\phi_{\text{LSCF}}(x)$  due to the system fluctuations, and the largest deviation in  $\phi(x)$ , defined as  $\max_{\{x\}} |\phi_{\text{FLMC}}(x) - \phi_{\text{LSCF}}(x)|$ , occurs at  $x = 3$  in all the cases, very close to the location (at  $x = 4$ ) of the maximum of  $\phi_{\text{LSCF}}(x)$ . Similar results are found at other  $\chi$ -values.

On the other hand, the FLMC results approach the LSCF predictions with increasing  $n$  at a given  $\chi$ , as expected. To quantitatively analyze the  $n$ -dependence of  $\phi(x)$ , we define  $\epsilon_\phi \equiv \sqrt{\sum_{x=1}^L [\phi_{\text{FLMC}}(x) - \phi_{\text{LSCF}}(x)]^2 / L}$  as in Paper II. Fig. 3(b) shows  $\epsilon_\phi$  as a function of  $n$  at various  $\chi$ . We see that  $\epsilon_\phi$  is larger in a poor solvent (i.e., at  $\chi = 1$  and 1.5) than in a good or  $\theta$ -solvent (i.e., at  $\chi = 0$  and 0.5), and that  $\epsilon_\phi \propto n^{-1}$  at large  $n$  for all the  $\chi$ -values.

The brush height is directly related to  $\phi(x)$ , i.e.,  $h = 2 \sum_{x=1}^L (x-1)\phi(x) / \bar{\phi}L$ . In the limit of  $\chi \rightarrow -\infty$ , all chains are fully stretched and LSCF theory gives the exact value of  $h = 39$  (for  $N = 40$ ). Fig. 4(a) shows that  $h_{\text{LSCF}}$  monotonically decreases with increasing  $\chi$ .

Fig. 4(b) shows that LSCF theory underestimates the brush height at any finite  $\chi \leq 1.5$ ; this is different from the brushes in an implicit, good solvent studied in Paper II, where LSCF theory overestimates  $h$  near the  $\theta$ -point.<sup>2</sup> We further see that  $h_{\text{FLMC}} - h_{\text{LSCF}}$  varies non-monotonically within the range of  $0 < \chi < 1$ . Similar to  $\epsilon_\phi$ , we also find that  $h_{\text{FLMC}} - h_{\text{LSCF}} \propto n^{-1}$  at large  $n$  for all the  $\chi$ -values (data not shown).

### 3.2.2 Free-end distribution and chain dimensions

Figs. 5(a) and 5(b) show  $\phi_{s=N}(x)$  obtained from canonical-ensemble simulations (denoted by  $\phi_{s=N,\text{FLMC}}(x)$ ) at  $\chi = 0$  and 1, respectively, along with the corresponding LSCF predictions (denoted by  $\phi_{s=N,\text{LSCF}}(x)$ ); note that  $\phi_{s=N}(x) = 0$  at odd  $x$  for chains of even  $N$  on the 1D lattice, and we omit such points in the figures. At  $\chi = 0$ , we see that  $\phi_{s=N,\text{FLMC}}(x) \propto \exp(kx/L)$  at small  $x$  and for small  $n$ . This exponential distribution of the free ends is also found in the 1D brushes in an implicit, good solvent studied in Paper II, and can be explained accordingly with an effective

value of  $(1 - 2\chi)N\bar{\phi} = 4$  for the parameter  $N/\kappa$  used in that paper, although at such a small value we cannot quantitatively predict  $k$ .<sup>2</sup> As also found in Paper II,  $\phi_{s=N,\text{FLMC}}(x) < \phi_{s=N,\text{LSCF}}(x)$  close to the substrate in all the cases. On the other hand, we find that  $\sqrt{\sum_{x=1}^L [\phi_{s=N,\text{FLMC}}(x) - \phi_{s=N,\text{LSCF}}(x)]^2} / L \propto n^{-1}$  at large  $n$  for all the  $\chi$ -values (data not shown), as in the case of  $\phi(x)$ .

The mean-square chain end-to-end distance  $R_e^2$  is directly related to  $\phi_{s=N}(x)$ , i.e.,  $R_e^2 = \sum_{x=1}^L (x-1)^2 \phi_{s=N}(x)$ . We find that both  $R_e^2$  and the mean-square chain radius of gyration  $R_g^2$  exhibits qualitatively the same behavior as  $h$ . That is, LSCF theory gives exact  $R_e^2 = 1521$  and  $R_g^2 = 133.25$  (for  $N = 40$ ) in the limit of  $\chi \rightarrow -\infty$ . With increasing  $\chi$ , both  $R_{e,\text{LSCF}}^2$  and  $R_{g,\text{LSCF}}^2$  monotonically decrease; note, however, that in the case of  $N = 40$  and  $\bar{\phi} = 0.1$  LSCF theory does not give the exact  $R_e^2$  and  $R_g^2$  in the limit of  $\chi \rightarrow \infty$  for finite  $n$  due to the chain correlations. On the other hand, LSCF theory underestimates  $R_e^2$  and  $R_g^2$  at any finite  $\chi \leq 1.5$ , and both  $R_{e,\text{FLMC}}^2 - R_{e,\text{LSCF}}^2$  and  $R_{g,\text{FLMC}}^2 - R_{g,\text{LSCF}}^2$  vary similarly to  $h_{\text{FLMC}} - h_{\text{LSCF}}$  shown in Fig. 4(b). Finally, Fig. 5(c) shows that  $R_{e,\text{FLMC}}^2 - R_{e,\text{LSCF}}^2 \propto n^{-1}$  at large  $n$  for all the  $\chi$ -values, and similar results are also found for  $R_g^2$  (data not shown).

### 3.3 Thermodynamic quantities

#### 3.3.1 Internal energy and specific heat

From Eqs. (8) and (10) we see that the internal energy per chain  $\beta u_c$  and the specific heat per chain  $C_v/k_B$  are directly related to  $\langle E \rangle / \rho_0^2$  and  $(\langle E^2 \rangle - \langle E \rangle^2) / \rho_0^4$ , respectively. Fig. 6(a) shows how  $E_{\text{LSCF}} / \rho_0^2$  and  $\beta u_{c,\text{LSCF}}$  vary with  $\chi$ . In the limit of  $\chi \rightarrow -\infty$ , the system is in the ground state with all chains fully stretched, and LSCF theory gives exact  $E = \beta u_c = 0$ . With increasing  $\chi$ ,  $E_{\text{LSCF}} / \rho_0^2$  monotonically increases and  $\beta u_{c,\text{LSCF}}$  exhibits a maximum around  $\chi = -6.3$ .

Fig. 6(b) shows  $(\langle E \rangle - E_{\text{LSCF}}) / \rho_0^2$  as a function of  $\chi$  for systems of various  $n$ , where  $\langle E \rangle$  is obtained from WL-TM simulations. In all the cases,  $(\langle E \rangle - E_{\text{LSCF}}) / \rho_0^2$  exhibits with increasing  $\chi$  a negative minimum followed by a positive maximum located at a  $\chi$ -value slightly larger than 0.5, and approaches 0 in the limit of  $\chi \rightarrow \infty$ . Following Paper II, we split  $(\langle E \rangle - E_{\text{LSCF}}) / \rho_0^2$  into two parts:  $\Delta\phi_1 \equiv \sum_{x=1}^L [\langle \hat{\rho}_{\text{FLMC}}^2(x) \rangle / \rho_0^2 - \phi_{\text{FLMC}}^2(x)]$  is the fluctuations of local segmental densities around their average in FLMC simulations, and  $\Delta\phi_2 \equiv \sum_{x=1}^L [\phi_{\text{FLMC}}^2(x) - \phi_{\text{LSCF}}^2(x)]$  is the difference between the square of the ensemble-averaged density profile in FLMC simulations and the corresponding LSCF

prediction. Both parts are due to the fluctuation effects neglected in LSCF theory.

Figs. 6(c) and 6(d) show that  $\Delta\phi_1 > 0$  and  $\Delta\phi_2 < 0$  at finite  $n$  and  $\chi \geq 0$ , which can be compared with Figs. 7(c) and 7(d) in Paper II, respectively. In fact, with the mapping of  $N/\kappa = (1 - 2\chi)N\bar{\phi}$ , the behavior of  $(\langle E \rangle - E_{\text{LSCF}})/\rho_0^2$  for  $-\infty < \chi \leq 0.5$  shown in Fig. 6(b) is qualitatively the same as Fig. 7(b) in Paper II. On the other hand, as revealed in Figs. 6(c) and 6(d), the decrease of  $(\langle E \rangle - E_{\text{LSCF}})/\rho_0^2$  from  $\chi = 0.5$  to 1 is due to the large decrease of  $\Delta\phi_2$ , which is similar to  $\epsilon_\phi$  shown in Fig. 3(b) since both measure the difference between  $\phi_{\text{FLMC}}(x)$  and  $\phi_{\text{LSCF}}(x)$ , and that from  $\chi = 1$  to 1.5 is due to the large decrease of  $\Delta\phi_1$ . Finally, Figs. 6(c) and 6(d) also show that both  $\Delta\phi_1$  and  $\Delta\phi_2$  are proportional to  $n^{-1}$  at large  $n$  for all the  $\chi$ -values, which leads to  $(\langle E \rangle - E_{\text{LSCF}})/\rho_0^2 \propto n^{-1}$  at large  $n$ .

With Eq. (8), we therefore have  $\beta u_{c,\text{FLMC}} - \beta u_{c,\text{LSCF}} = 0$  at  $\chi = 0$  and in the limits of  $\chi \rightarrow \pm\infty$ . Fig. 6(e) shows  $\beta u_{c,\text{FLMC}} - \beta u_{c,\text{LSCF}}$  as a function of  $\chi$  for systems of various  $n$ , which can be easily understood based on the above analysis. In particular, at finite  $\chi > 0$ , LSCF theory overestimates the internal energy per chain and its prediction is approached by FLMC results at a rate of  $1/n$  at large  $n$ .

Fig. 7(a) shows  $(\langle E^2 \rangle - \langle E \rangle^2)/\rho_0^4$  as a function of  $\chi$  for systems of various  $n$  obtained from FLMC simulations; note that the LSCF prediction is 0 regardless of  $\chi$ . We see that  $(\langle E^2 \rangle - \langle E \rangle^2)/\rho_0^4$  exhibits a maximum at  $\chi \approx 0.9$ . In the limits of  $\chi \rightarrow -\infty$  and  $\infty$ , the system is in the ground state of  $E = 0$  and the ‘‘ceiling’’ state of  $E = 360n^2$  (for  $\bar{\phi} = 0.1$  and  $N = 40$ ), respectively, with no fluctuations, thus  $(\langle E^2 \rangle - \langle E \rangle^2)/\rho_0^4 = 0$ . Fig. 7(b) shows the  $n$ -dependence of  $(\langle E^2 \rangle - \langle E \rangle^2)/\rho_0^4$  at various  $\chi$  obtained from canonical-ensemble simulations, where we see that  $(\langle E^2 \rangle - \langle E \rangle^2)/\rho_0^4 \propto n^{-1}$  at large  $n$  for all the  $\chi$ -values.

With Eq. (10), we therefore have  $C_v/k_B = 0$  at  $\chi = 0$  and in the limits of  $\chi \rightarrow \pm\infty$ , and  $> 0$  at other  $\chi$ -values. LSCF theory gives  $C_v/k_B = 0$  regardless of  $\chi$ , which, for any finite  $\chi > 0$ , is approached by FLMC results at a rate of  $1/n$  at large  $n$  (data not shown).

### 3.3.2 Free energy and entropy

Similar to Papers I and II, here we compare the differences in free energy per chain,  $\Delta f_c \equiv f_c(\chi) - f_c(\chi \rightarrow -\infty)$ , and in entropy per chain,  $\Delta s_c \equiv s_c(\chi) - s_c(\chi \rightarrow -\infty)$ , from the reference state in the limit of  $\chi \rightarrow -\infty$ , where all chains are fully stretched. Note that, for any finite  $n_S$ -value, while LSCF theory does not give the exact  $f_c$  and  $s_c$

in this reference state due to the correlations among solvent molecules caused by the incompressibility constraint, the deviations from the exact value are known analytically (see Eqs. (26) and (27)).

Fig. 8(a) shows how the LSCF predictions of  $\beta\Delta f_{c,\text{LSCF}}$  and  $\Delta s_{c,\text{LSCF}}/k_B$  vary with  $\chi$ . With increasing  $\chi$ ,  $\beta\Delta f_{c,\text{LSCF}}$  monotonically decreases but  $\Delta s_{c,\text{LSCF}}/k_B$  exhibits a maximum at  $\chi = 0$ ; the latter is a general feature for all  $N$ , as shown in Appendix B. In the limit of  $\chi \rightarrow \infty$ ,  $\beta\Delta f_{c,\text{LSCF}}$  approaches  $-\infty$  but  $\Delta s_{c,\text{LSCF}}/k_B$  approaches a finite value.

Fig. 8(b) shows that  $\beta(\Delta f_{c,\text{FLMC}} - \Delta f_{c,\text{LSCF}})$  exhibits a maximum at a negative  $\chi$ -value (which decreases with increasing  $n$ ), crosses 0 at a  $\chi$ -value between 0.5 and 0.8, and seems to approach a negative constant in the limit of  $\chi \rightarrow \infty$  at any finite  $n$ . LSCF theory therefore underestimates  $\Delta f_c$  at small  $\chi \geq 0$  and overestimates it at larger  $\chi$  at finite  $n$ . Fig. 8(c) shows that, while  $\beta|\Delta f_{c,\text{FLMC}} - \Delta f_{c,\text{LSCF}}| \propto n^{-1}$  seems to hold for all  $n$  at  $\chi = 0$  as well as at large  $n$  for large  $\chi$ -values (e.g., 1.5), it may not hold even at large  $n$  for intermediate  $\chi$ -values (e.g., 0.5 and 1) near which  $\Delta f_{c,\text{FLMC}}$  coincides with  $\Delta f_{c,\text{LSCF}}$ .

With Eq. (9), the behavior of  $-(\Delta s_{c,\text{FLMC}} - \Delta s_{c,\text{LSCF}})/k_B$  shown in Fig. 8(d) can be readily understood. We see that, with increasing  $\chi$ ,  $-(\Delta s_{c,\text{FLMC}} - \Delta s_{c,\text{LSCF}})/k_B$  exhibits two maxima, one at a negative  $\chi$ -value (which decreases with increasing  $n$ ) and the other at a  $\chi$ -value slightly larger than 0.5; these locations coincide with the corresponding extremum of  $(\langle E \rangle - E_{\text{LSCF}})/\rho_0^2$  in Fig. 6(b), which is a general feature for all  $n$  and  $N$  as shown in Appendix C.  $-(\Delta s_{c,\text{FLMC}} - \Delta s_{c,\text{LSCF}})/k_B$  then crosses 0 at a larger  $\chi$ , and approaches the same negative constant as  $\beta(\Delta f_{c,\text{FLMC}} - \Delta f_{c,\text{LSCF}})$  does in the limit of  $\chi \rightarrow \infty$  at any finite  $n$ . LSCF theory therefore overestimates  $\Delta s_c$  at small  $\chi \geq 0$  and underestimates it at larger  $\chi$  at finite  $n$ . In addition,  $-(\Delta s_{c,\text{FLMC}} - \Delta s_{c,\text{LSCF}})/k_B$  exhibits a local minimum at  $\chi = 0$ , which is a general feature of the brushes in an explicit solvent for all  $n$  and  $N$  as shown in Appendix C but not seen in the brushes in an implicit solvent studied in Paper II.

Finally, Fig. 8(e) shows that, while  $|\Delta s_{c,\text{FLMC}} - \Delta s_{c,\text{LSCF}}|/k_B \propto n^{-1}$  seems to hold for all  $n$  at  $\chi = 0$  and 0.5, it may not hold even at large  $n$  for  $\chi$ -values (e.g., 1 and 1.5) near which  $\Delta s_{c,\text{FLMC}}$  coincides with  $\Delta s_{c,\text{LSCF}}$ .

## 4 Summary

Using fast lattice Monte Carlo (FLMC) simulations<sup>3</sup> both in a canonical ensemble and with Wang-Landau-Transition-Matrix (WL-TM) sampling,<sup>46–48</sup> we have studied a 1D model system of laterally homogeneous homopolymer brushes in an explicit solvent with Kronecker  $\delta$ -function interactions. The fluctuations and correlations in this system are controlled by a few physical parameters: the chain length  $N$ , the average polymer volume fraction  $\bar{\phi}$ , the Flory-Huggins interaction parameter  $\chi$  between polymer segments and solvent molecules, and the number of grafted chains  $n$ . Direct comparisons of the simulation results with those from the corresponding lattice self-consistent field (LSCF) theory, both of which are based on the *same* Hamiltonian (thus without any parameter-fitting between them), unambiguously and quantitatively reveal the fluctuations and correlations in the system. This is the third paper in our series of studies with similar methodology and purpose, and extends our previous work on the brushes in an implicit, good solvent reported in the preceding paper in this series<sup>2</sup> (referred as Paper II). Such direct comparisons distinguish our work from all previously reported comparisons between SCF theories and molecular simulations of homopolymer brushes,<sup>9, 23, 25, 26, 31–33, 35–37, 43, 45</sup> where different models were used in the theories and simulations.

We have examined in detail how  $\chi$  and  $n$  affect both the brush structures (including the ensemble-averaged segmental density profile  $\phi(x)$  and free-end distribution  $\phi_{s=N}(x)$ , where  $x$  denotes the direction perpendicular to the grafting substrate, as well as the related brush height  $h$ , mean-square chain end-to-end distance  $R_e^2$  and radius of gyration  $R_g^2$ ) and various thermodynamic quantities (including the canonical-ensemble average of energy level  $\langle E \rangle$  and the related internal energy per chain of length  $N$  (i.e., per  $N$  lattice sites)  $u_c$ , the fluctuations of energy level  $\langle E^2 \rangle - \langle E \rangle^2$  and the related specific heat per chain  $C_v$ , the difference in free-energy per chain  $\Delta f_c \equiv f_c(\chi) - f_c(\chi \rightarrow -\infty)$  and that in entropy per chain  $\Delta s_c \equiv s_c(\chi) - s_c(\chi \rightarrow -\infty)$  from the reference state in the limit of  $\chi \rightarrow -\infty$  where all chains are fully stretched). Such thermodynamic quantities were not examined in previous comparisons of homopolymer brushes. While most results presented here are for  $N = 40$  and  $\bar{\phi} = 0.1$ , similar results are found for other values of  $N$  and  $\bar{\phi}$ .

For systems at finite  $n$ , we find that LSCF theory gives exact results for all the above quantities in the limit of  $\chi \rightarrow -\infty$ , where the system is in the ground state of  $E = 0$  (i.e., no fluctuations) with all chains having the same conformation (i.e., no chain correlations). LSCF theory, however, neglects the correlations among solvent molecules caused by the incompressibility constraint, thus overestimating the solvent entropy; this

is different from the brushes in an implicit, good solvent studied in Paper II.

At finite  $n$  and  $\chi$ , the segmental density profile obtained from FLMC simulations  $\phi_{\text{FLMC}}(x)$  is flatter than the LSCF prediction  $\phi_{\text{LSCF}}(x)$ . The largest deviation between the two profiles occurs close to the grafting substrate where  $\phi_{\text{LSCF}}(x)$  is almost at its maximum, and the mean-square difference between them is larger in a poor solvent than in a good or  $\theta$ -solvent. Close to the substrate, the free-end density from FLMC simulations  $\phi_{s=N,\text{FLMC}}(x)$  is lower than the LSCF prediction  $\phi_{s=N,\text{LSCF}}(x)$ . LSCF theory underestimates  $h$ ,  $R_e^2$  and  $R_g^2$  at any finite  $\chi \leq 1.5$ , different from the brushes in an implicit, good solvent studied in Paper II.

Regarding the thermodynamic quantities, since  $\langle E \rangle / \rho_0^2 \equiv \sum_x [\phi(x) - \bar{\phi}]^2 = -\beta u_c / (\chi N / V)$  and  $C_v / k_B = [(\chi N)^2 \rho_0 / V N] (\langle E^2 \rangle - \langle E \rangle^2) / \rho_0^4$ , where  $\rho_0 = nN / \bar{\phi} V$  is the average number density of polymer segments and solvent molecules and  $V$  the total number of lattice sites ( $= N$  for our 1D brushes), understanding the behavior of  $\langle E \rangle$  and  $\langle E^2 \rangle - \langle E \rangle^2$  is crucial for understanding that of  $u_c$  and  $C_v$ . As expected,  $E_{\text{LSCF}}$  monotonically increases while  $\beta u_{c,\text{LSCF}}$  monotonically decreases with increasing  $\chi \geq 0$ . We find that  $(\langle E \rangle - E_{\text{LSCF}}) / \rho_0^2$  exhibits with increasing  $\chi$  a negative minimum followed by a positive maximum located at a  $\chi$ -value slightly larger than 0.5, and approaches 0 in the limit of  $\chi \rightarrow \infty$ . Following Paper II we split it into two parts:  $\Delta\phi_1$  is the fluctuations of local segmental densities around their average in FLMC simulations, and  $\Delta\phi_2$  is the difference between the square of the ensemble-averaged density profile in FLMC simulations and the corresponding LSCF prediction. Both parts are due to fluctuations neglected in LSCF theory, and  $\Delta\phi_2$  is unique for inhomogeneous systems. We find that  $\Delta\phi_1 > 0$  and  $\Delta\phi_2 < 0$  at finite  $n$  and  $\chi \geq 0$ . We also see that  $(\langle E^2 \rangle - \langle E \rangle^2) / \rho_0^4$  exhibits a maximum at  $\chi \approx 0.9$ . It is trivial that LSCF theory gives exact results of  $\beta u_c = 0$  and  $C_v / k_B = 0$  at  $\chi = 0$  and in the limit of  $\chi \rightarrow -\infty$ , as well as that of  $C_v / k_B = 0$  in the limit of  $\chi \rightarrow \infty$ . At finite  $\chi > 0$ , LSCF theory overestimates  $\beta u_c$  and underestimates  $C_v / k_B$ .

On the other hand, while  $\beta \Delta f_{c,\text{LSCF}}$  monotonically decreases with increasing  $\chi$ ,  $\Delta s_{c,\text{LSCF}} / k_B$  exhibits a maximum at  $\chi = 0$  as proved in Appendix B. In the limit of  $\chi \rightarrow \infty$ ,  $\beta \Delta f_{c,\text{LSCF}}$  approaches  $-\infty$  but  $\Delta s_{c,\text{LSCF}} / k_B$  approaches a finite value. At finite  $n$ , while  $\beta (\Delta f_{c,\text{FLMC}} - \Delta f_{c,\text{LSCF}})$  monotonically decreases with increasing  $\chi \geq 0$ ,  $-(\Delta s_{c,\text{FLMC}} - \Delta s_{c,\text{LSCF}}) / k_B$  exhibits a local minimum at  $\chi = 0$  and a local maximum at a  $\chi$ -value slightly larger than 0.5; the location of the latter coincides with the corresponding extremum of  $(\langle E \rangle - E_{\text{LSCF}}) / \rho_0^2$ , as proved in Appendix C. Both  $\beta (\Delta f_{c,\text{FLMC}} - \Delta f_{c,\text{LSCF}})$

and  $-(\Delta s_{c,\text{FLMC}} - \Delta s_{c,\text{LSCF}})/k_B$  then cross 0 at a larger  $\chi$ , and approach the same constant in the limit of  $\chi \rightarrow \infty$ . At finite  $n$ , LSCF theory therefore underestimates  $\Delta f_c$  but overestimates  $\Delta s_c$  at small  $\chi \geq 0$ , and the opposite occurs at larger  $\chi$ .

At finite  $\chi \geq 0$ , FLMC results approach LSCF predictions at a rate of  $1/n$  at large  $n$ . This scaling has also been found in our previous work.<sup>1-3</sup> As expected, LSCF theory is exact in the limit of  $n \rightarrow \infty$ , where there are no fluctuations or correlations. For the homopolymer brushes studied here, however, this scaling does not hold for certain quantities close to the finite  $\chi$ -values at which the FLMC results coincide with LSCF predictions, e.g.,  $\Delta f_c$  and  $\Delta s_c$  at  $\chi$ -values somewhat larger than 0.5 (see Figs. 8(b) and 8(d)).

Finally, when  $\phi(x) \ll 1$  for all  $x$ , there is an approximate correspondence between brushes in an explicit solvent studied here and those in an implicit, good solvent studied in Paper II, where a parameter  $\kappa$  inversely proportional to the second virial coefficient was used to characterize the solvent quality. Most results for  $\chi \leq 0.5$  reported here can therefore be qualitatively understood based on Paper II, with  $(1 - 2\chi)\bar{\phi}$  and  $\phi(x)/\bar{\phi}$  here corresponding to  $\kappa$  and  $\phi(x)$  in that work. This correspondence is independent of the system dimensionality and whether or not the chains are grafted, as shown in Appendix A.

## Acknowledgement

BL acknowledges the financial support for this work provided by the National Science Fund for Distinguished Young Scholars of China (No. 20925414), and QW acknowledges the financial support provided by NSF CAREER Award CBET-0847016.

# Appendix

## A. Correspondence between brushes in explicit and implicit solvents

When  $\hat{\rho}(x) \ll \rho_0$  (i.e.,  $\phi(x) \ll 1$ ) for all  $x$ , there is an approximate correspondence between brushes in explicit and implicit solvents. In this case, Eq. (3) can be re-written as

$$\begin{aligned}
\mathcal{Z} &= \frac{1}{n!} \prod_{k=1}^n \prod_{s=1}^N \sum_{X_{k,s}} \cdot \exp \left\{ -\beta \sum_{k=1}^n h_k^C + \frac{\chi}{\rho_0} E - \sum_x \ln [\rho_0 - \hat{\rho}(x)]! \right\} \\
&\sim \frac{1}{n!} \prod_{k=1}^n \prod_{s=1}^N \sum_{X_{k,s}} \cdot \exp \left\{ -\beta \sum_{k=1}^n h_k^C + \frac{\chi}{\rho_0} E - \sum_x [\rho_0 - \hat{\rho}(x)] \ln [\rho_0 - \hat{\rho}(x)] \right\} \\
&\sim \frac{1}{n!} \prod_{k=1}^n \prod_{s=1}^N \sum_{X_{k,s}} \cdot \exp \left\{ -\beta \sum_{k=1}^n h_k^C + \frac{\chi}{\rho_0} E + \sum_x [\rho_0 - \hat{\rho}(x)] \left[ \frac{\hat{\rho}(x)}{\rho_0} + \frac{\hat{\rho}^2(x)}{2\rho_0^2} \right] \right\} \\
&\sim \frac{1}{n!} \prod_{k=1}^n \prod_{s=1}^N \sum_{X_{k,s}} \cdot \exp \left\{ -\beta \sum_{k=1}^n h_k^C - \left( \frac{1}{2} - \chi \right) \bar{\phi} \frac{E}{\bar{\phi}\rho_0} \right\} \tag{29}
\end{aligned}$$

where we have used the Stirling approximation and the Taylor expansion  $\ln(1-a) \approx -a - a^2/2$  for small  $a$ , “ $\sim$ ” indicates that a constant in the Hamiltonian is further neglected, and to obtain the last line the  $O(\hat{\rho}^3(x))$ -term is also neglected. Comparing the above to Eqs. (1) and (2) in Paper II and noting that  $\bar{\phi}\rho_0 = nN/V$  here corresponds to  $\rho_0$  in Paper II, we see that  $(1-2\chi)N\bar{\phi}$  and  $\tilde{\phi}(x) \equiv \phi(x)/\bar{\phi}$  here correspond to  $N/\kappa$  and  $\phi(x)$  in Paper II, respectively. We note that this correspondence is actually independent of the system dimensionality and whether or not the chains are grafted.

This correspondence can also be seen in LSCF calculations. Using the Taylor expansion in Eq. (22) and defining  $i\tilde{\omega}(x) \equiv i\omega(x) + \chi N(2\bar{\phi} - 1) - N\bar{\phi}$ , we have

$$i\tilde{\omega}(x) \approx (1 - 2\chi)N\bar{\phi}[\tilde{\phi}(x) - 1] \tag{30}$$

With the definitions of  $\tilde{q}_t^*(x) \equiv q_t^*(x) \exp[-\chi(2\bar{\phi} - 1)t + \bar{\phi}t]$  and  $\tilde{q}_s(x) \equiv q_s(x) \exp[-\chi(2\bar{\phi} - 1)s + \bar{\phi}s]$ , which satisfy the same recursive relations as Eqs. (20) and (21) with  $i\omega(x)$  there replaced by  $i\tilde{\omega}(x)$ , Eq. (17) becomes

$$\tilde{\phi}_s(x) = \frac{\exp[i\tilde{\omega}(x)/N]}{\tilde{q}_N^*(x=1)} \tilde{q}_s(x) \tilde{q}_{N+1-s}^*(x) \tag{31}$$

with  $\tilde{\phi}_s(x) \equiv \phi_s(x)/\bar{\phi}$ . Comparing Eqs. (30) and (31) with Eqs. (12) and (14) in Paper II, we see that, in addition to the aforementioned correspondence,  $i\tilde{\omega}(x)$ ,  $\tilde{q}_t^*(x)$ ,  $\tilde{q}_s(x)$  and  $\tilde{\phi}_s(x)$  here correspond to  $i\omega(x)$ ,  $q_t^*(x)$ ,  $q_s(x)$  and  $\phi_s(x)$  in Paper II, respectively.

To quantify the difference in polymer segmental density profile between brushes in an implicit and an explicit solvent, Fig. 9 shows  $\Delta\phi \equiv \sqrt{\sum_x [\phi^{\text{Ex}}(x)/\bar{\phi} - \phi^{\text{Im}}(x)]^2}/L$  as a function of  $\bar{\phi}$  for  $N = 40$ , where  $\phi^{\text{Ex}}(x)$  and  $\phi^{\text{Im}}(x)$  denote, respectively, the polymer segmental density profile obtained from LSCF calculations of brushes in an explicit and an implicit solvent on the 1D lattice, with  $N/\kappa = (1 - 2\chi)N\bar{\phi}$  used in the latter.<sup>2</sup> We see that  $\Delta\phi$  increases with increasing  $\bar{\phi}$  as expected, and that  $\Delta\phi \propto \bar{\phi}^2$  at small  $\bar{\phi}$ . In addition,  $\Delta\phi$  is larger in a solvent of better quality.

Finally, the shift of  $i\omega(x)$  to  $i\tilde{\omega}(x)$  gives  $\tilde{Q} \equiv \tilde{q}_N^*(x=1)/L = Q \exp[-\chi N(2\bar{\phi} - 1) + N\bar{\phi}]$ . With this and the Taylor expansion, Eq. (23) gives

$$\begin{aligned} \beta f_{c,\text{LSCF}} = & \frac{\bar{\phi}}{2L} (1 - 2\chi) N \bar{\phi} \sum_x [1 - \tilde{\phi}^2(x)] - \bar{\phi} \ln \tilde{Q} [i\tilde{\omega}] - \bar{\phi} \frac{\ln(G^n/n!)}{n} \\ & + \frac{\bar{\phi}}{n} \ln n_S! - N(1 - \bar{\phi}) \ln V \end{aligned} \quad (32)$$

For homopolymer brush in an implicit, good solvent, Eqs. (19) and (28) in Paper II give

$$\beta f_{c,\text{LSCF}} = \frac{1}{2L} \frac{N}{\kappa} \sum_{x=1}^L [1 - \phi^2(x)] - \ln Q [i\omega] - \frac{\ln(G^n/n!)}{n} \quad (33)$$

Comparing these two equations, we see that  $\beta f_c/\bar{\phi}$  in an explicit solvent corresponds to  $\beta f_c$  in an implicit, good solvent; the last two terms in Eq. (32) correspond to the solvent entropy.

Our FLMC and LSCF results for brushes in an explicit, good solvent reported here can therefore be qualitatively understood based on those for brushes in an implicit, good solvent reported in Paper II. Note, however, that the reference state used for  $\Delta f_c$  and  $\Delta s_c$  here (i.e., the limit of  $\chi \rightarrow -\infty$ ) is different from that used in Paper II (i.e.,  $N/\kappa = 0$ ); for our model system studied in Paper II,  $\beta [f_c(N/\kappa \rightarrow \infty) - f_c(N/\kappa = 0)] = -[s_c(N/\kappa \rightarrow \infty) - s_c(N/\kappa = 0)]/k_B = 24.956$  for chains of  $N = 40$ .

## B. The maximum of $\Delta s_{c,\text{LSCF}}/k_B$ at $\chi = 0$

At given  $N$  and  $\bar{\phi}$ ,  $s_{c,\text{LSCF}}$  can be obtained from Eqs. (9) and (23) as

$$\frac{s_{c,\text{LSCF}} - s_c^{id}}{k_B} = \chi N \bar{\phi} - 2\chi \sum_x \phi^2(x) - \sum_x \ln[1 - \phi(x)] + N(1 - \bar{\phi}) \ln(1 - \bar{\phi}) + \bar{\phi} \ln Q \quad (34)$$

which gives

$$\frac{d}{d\chi} \left( \frac{s_{c,\text{LSCF}} - s_c^{id}}{k_B} \right) = \bar{\phi} N - \sum_x \left[ 2\phi^2(x) + \left( 4\chi\phi(x) - \frac{1}{1 - \phi(x)} \right) \frac{d\phi(x)}{d\chi} \right] + \bar{\phi} \frac{d \ln Q}{d\chi} \quad (35)$$

With  $\frac{\delta \ln Q}{\delta i\omega} = -\phi(x)/N\bar{\phi}$  (i.e., Eqs. (16) and (17)) and Eq. (22), we have

$$\bar{\phi} \frac{d \ln Q}{d\chi} = \bar{\phi} \sum_x \frac{\delta \ln Q}{\delta i\omega(x)} \frac{di\omega(x)}{d\chi} = \sum_x \left[ -\frac{\phi(x)}{1 - \phi(x)} \frac{d\phi(x)}{d\chi} + 2\phi^2(x) + 2\chi\phi(x) \frac{d\phi(x)}{d\chi} \right] - \bar{\phi} L \quad (36)$$

We therefore obtain

$$\frac{d}{d\chi} \left( \frac{s_{c,\text{LSCF}} - s_c^{id}}{k_B} \right) = -2\chi \sum_x \phi(x) \frac{d\phi(x)}{d\chi} \quad (37)$$

which gives

$$\left. \frac{d}{d\chi} \left( \frac{s_{c,\text{LSCF}} - s_c^{id}}{k_B} \right) \right|_{\chi=0} = 0 \quad (38)$$

and

$$\left. \frac{d^2}{d\chi^2} \left( \frac{s_{c,\text{LSCF}} - s_c^{id}}{k_B} \right) \right|_{\chi=0} = -2 \sum_x \phi(x) \frac{d\phi(x)}{d\chi} \Big|_{\chi=0} = -\frac{d}{d\chi} \sum_x [\phi(x) - \bar{\phi}]^2 \Big|_{\chi=0} < 0 \quad (39)$$

where the last inequality results from the fact that  $\sum_x [\phi(x) - \bar{\phi}]^2$  is a monotonically increasing function of  $\chi$ .  $(s_{c,\text{LSCF}} - s_c^{id})/k_B$  therefore exhibits a maximum at  $\chi = 0$ , so does  $\Delta s_{c,\text{LSCF}}/k_B$ .

## C. Extrema of $-(\Delta s_{c,\text{FLMC}} - \Delta s_{c,\text{LSCF}})/k_B$ and $(\langle E \rangle - E_{\text{LSCF}})/\rho_0^2$

From Eqs. (6)~(9), we have at given  $n$ ,  $N$  and  $\bar{\phi}$

$$\frac{s_{c,\text{FLMC}}(\chi)}{k_B} = -\frac{\chi}{\rho_0} \frac{d \ln \mathcal{Z}}{d\chi} + \frac{1}{\rho_0} \ln \mathcal{Z} \quad (40)$$

and

$$\frac{\langle E(\chi) \rangle}{\rho_0^2} = \frac{1}{\rho_0} \frac{d \ln \mathcal{Z}}{d\chi} \quad (41)$$

With Eq. (37) we therefore obtain

$$\begin{aligned} \frac{d}{d\chi} \left[ -\frac{s_{c,\text{FLMC}} - (s_{c,\text{LSCF}} - s_c^{id})}{k_B} \right] &= \chi \frac{d}{d\chi} \left( \frac{\langle E \rangle - E_{\text{LSCF}}}{\rho_0^2} \right) \\ &= -\frac{\chi}{\rho_0} \frac{d^2 \ln \mathcal{Z}}{d\chi^2} + 2\chi \sum_x \phi(x) \frac{d\phi(x)}{d\chi} \end{aligned} \quad (42)$$

which indicates that the extrema of  $(\langle E \rangle - E_{\text{LSCF}})/\rho_0^2$  have the same location as those of  $-[s_{c,\text{FLMC}} - (s_{c,\text{LSCF}} - s_c^{id})]/k_B$  (or equivalently  $-(\Delta s_{c,\text{FLMC}} - \Delta s_{c,\text{LSCF}})/k_B$ ), and that the latter has an additional extremum at  $\chi = 0$ . Furthermore, at the extrema of  $(\langle E \rangle - E_{\text{LSCF}})/\rho_0^2$ ,

$$\frac{d^2}{d\chi^2} \left[ -\frac{s_{c,\text{FLMC}} - (s_{c,\text{LSCF}} - s_c^{id})}{k_B} \right] = \chi \frac{d^2}{d\chi^2} \left( \frac{\langle E \rangle - E_{\text{LSCF}}}{\rho_0^2} \right) \quad (43)$$

which indicates that both  $(\langle E \rangle - E_{\text{LSCF}})/\rho_0^2$  and  $-[s_{c,\text{FLMC}} - (s_{c,\text{LSCF}} - s_c^{id})]/k_B$  (or equivalently  $-(\Delta s_{c,\text{FLMC}} - \Delta s_{c,\text{LSCF}})/k_B$ ) reach either local maximum or local minimum at  $\chi > 0$ , but one of them reaches local maximum while the other reaches local minimum at  $\chi < 0$ . Due to the  $\ln \mathcal{Z}$ -term involved, however, it is difficult to tell whether these extrema are local maxima or minima.

## References

- [1] Zhang, P.; Zhang, X.; Li, B.; Wang, Q. *Soft Matter* **2011**, *7*, 4461.
- [2] Zhang, P.; Li, B.; Wang, Q. *Macromolecules* **2011**, *44*, 7837.
- [3] Wang, Q. *Soft Matter* **2009**, *5*, 4564; *ibid.* **2010**, *6*, 6206.
- [4] Fredrickson, G. H. *The Equilibrium Theory of Inhomogeneous Polymers*, **2006**, Oxford University Press.
- [5] Whitmore, M. D.; Noolandi, J. *Macromolecules* **1990**, *23*, 3321.
- [6] Baranowski, R.; Whitmore, M. D. *J. Chem. Phys.* **1995**, *103*, 2343.
- [7] Baranowski, R.; Whitmore, M. D. *J. Chem. Phys.* **1998**, *108*, 9885.
- [8] Whitmore, M. D.; Baranowski, R. *Macromol. Theory Simul.* **2005**, *14*, 75.
- [9] Pepin, M. P.; Whitmore, M. D. *J. Chem. Phys.* **1999**, *111*, 10381.
- [10] Skvortsov, A. M.; Pavlushkov, I. V.; Gorbunov, A. A.; Zhulina, E. B.; Borisov, O. V.; Pryamitsyn, V. A. *Polym. Sci. USSR* **1988**, *30*, 1706.
- [11] Zhulina, E. B.; Borisov, O. V.; Pryamitsyn, V. A.; Birshtein, T. M. *Macromolecules* **1991**, *24*, 140.
- [12] Shim, D. F. K.; Cates, M. E. *J. Phys.-Paris* **1989**, *50*, 3535.
- [13] Amoskov, V. M.; Pryamitsyn, V. A. *J. Chem. Soc. Faraday T.* **1994**, *90*, 889.
- [14] Amoskov, V. M.; Pryamitsyn, V. A. *Polym. Sci. Ser. A* **1995**, *37*, 731.
- [15] Amoskov, V. M.; Pryamitsyn, V. A. *Macromol. Theory Simul.* **2003**, *12*, 223.
- [16] Cosgrove, T.; Heath, T.; Vanlent, B.; Leermakers, F.; Scheutjens, J. *Macromolecules* **1987**, *20*, 1692.
- [17] Gorbunov, A. A.; Pavlushkov, I. V.; Skvortsov, A. M. *Polym. Sci. USSR* **1988**, *30*, 414.
- [18] Skvortsov, A. M.; Pavlushkov, I. V.; Gorbunov, A. A. *Polym. Sci. USSR* **1988**, *30*, 487.

- [19] Hirz, S. J. *Masters Thesis*, **1986**, University of Minnesota.
- [20] Huang, K. L.; Balazs, A. C. *Macromolecules* **1993**, *26*, 4736.
- [21] Martin, J. I.; Wang, Z. G. *J. Phys. Chem.* **1995**, *99*, 2833.
- [22] Wijmans, C. M.; Scheutjens, J.; Zhulina, E. B. *Macromolecules* **1992**, *25*, 2657.
- [23] Chakrabarti, A.; Toral, R. *Macromolecules* **1990**, *23*, 2016.
- [24] Milik, M.; Kolinski, A.; Skolnick, J. *J. Chem. Phys.* **1990**, *93*, 4440.
- [25] Lai, P. Y.; Binder, K. *J. Chem. Phys.* **1991**, *95*, 9288.
- [26] Lai, P. Y.; Binder, K. *J. Chem. Phys.* **1992**, *97*, 586.
- [27] Pakula, T. *Macromol. Symp.* **1999**, *139*, 49.
- [28] Huh, J.; Ahn, C. H.; Jo, W. H.; Bright, J. N.; Williams, D. R. M. *Macromolecules* **2005**, *38*, 2974.
- [29] Ohno, K.; Sakamoto, T.; Minagawa, T.; Okabe, Y. *Macromolecules* **2007**, *40*, 723.
- [30] Coluzza, I.; Hansen, J. P. *Phys. Rev. Lett.* **2008**, *100*, 016104.
- [31] Karaiskos, E.; Bitsanis, I. A.; Anastasiadis, S. H. *J. Polym. Sci., Part B: Polym. Phys.* **2009**, *47*, 2449.
- [32] Murat, M.; Grest, G. S. *Macromolecules* **1989**, *22*, 4054.
- [33] Grest, G. S.; Murat, M. *Macromolecules* **1993**, *26*, 3108.
- [34] Grest, G. S. *Macromolecules* **1994**, *27*, 418.
- [35] Seidel, C.; Netz, R. R. *Macromolecules* **2000**, *33*, 634.
- [36] Kreer, T.; Metzger, S.; Muller, M.; Binder, K.; Baschnagel, J. *J. Chem. Phys.* **2004**, *120*, 4012.
- [37] He, G. L.; Merlitz, H.; Sommer, J. U.; Wu, C. X. *Macromolecules* **2007**, *40*, 6721.
- [38] Dimitrov, D. I.; Milchev, A.; Binder, K. *J. Chem. Phys.* **2007**, *127*, 084905.
- [39] He, G. L.; Merlitz, H.; Sommer, J. U.; Wu, C. X. *Eur. Phys. J. E* **2007**, *24*, 325.

- [40] Neelov, I. M.; Binder, K. *Macromol. Theory Simul.* **1995**, *4*, 119.
- [41] Pal, S.; Seidel, C. *Macromol. Theory Simul.* **2006**, *15*, 668.
- [42] Weinhold, J. D.; Kumar, S. K. *J. Chem. Phys.* **1994**, *101*, 4312.
- [43] Laradji, M.; Guo, H.; Zuckermann, M. J. *Phys. Rev. E* **1994**, *49*, 3199.
- [44] Soga, K. G.; Guo, H.; Zuckermann, M. J. *Europhys. Lett.* **1995**, *29*, 531.
- [45] Lai, P. Y.; Zhulina, E. B. *J. Phys. II* **1992**, *2*, 547.
- [46] Shell, M. S.; Debenedetti, P. G.; Panagiotopoulos, A. Z. *J. Chem. Phys.* **2003**, *119*, 9406.
- [47] Ghulghazaryan, R. G.; Hayryan, S.; Hu, C. *J. Comput. Chem.* **2007**, *28*, 715.
- [48] Chap. 3 in Chipot C.; Pohorille A. (Ed.) *Free Energy Calculations: Theory and Applications in Chemistry and Biology*, **2007**, Springer.
- [49] Yang, D.; Wang, Q. *J. Chem. Phys.*, to be submitted.
- [50] Frenkel, D.; Smit, B. *Understanding Molecular Simulation – From Theory to Applications*, **2002**, Academic Press.
- [51] Press, W. H.; Teukolsky, S. A.; Vetterling, W. T.; Flannery, B. P. *Numerical Recipes in FORTRAN: the Art of Scientific Computing*, **2002**, Cambridge University Press.
- [52] Different from Eq. (22), this is the case when  $\phi \cdot i\omega$  is set to be 0, as can be seen from Eq. (12).
- [53] Yeung, C.; Balazs, A. C.; Jasnow, D. *Macromolecules* **1994**, *26*, 1914.
- [54] Roderick, C.; Guo, H.; and Zuckermann, M. J. *Phys. Rev. E* **2000**, *63*, 012501.

## List of Figures

**Figure 1.**(a) Density of states  $g(E)$  estimated by WL-TM simulations for  $n \geq 2$  and the exact  $g(E)$  for  $n = 1$  obtained by enumeration; (b) the normalized probability distribution function  $P(E, \chi)$  at  $\chi = 0$  and 1.5 for  $n = 1$  and 16. Note that  $g(E) = 0$  for odd  $E$  and we omit such points, as well as those points at large  $E$  where  $g(E) = 0$ , besides,  $g(E = 0) = 1$  for system with different  $n$ .  $L = N = 40$  and  $\bar{\phi}_A = 0.1$  is used here.

**Figure 2.**(a) Log-log plot of the error per energy level  $\epsilon$  and the related error in the free energy per chain,  $\epsilon_f$ , at  $\chi = 0, 1.0, 1.5$  as a function of the number of Monte Carlo steps of the Transition-Matrix sampling, TM MCS, in our WL-TM simulations of the single-chain system.  $L = N = 40$  and  $\bar{\phi} = 0.1$  is used here. (b) the difference of free energy per chain between the WL-TM algorithm and the enumeration for the single-chain system as a function of  $\chi$ , where the WL-TM simulation results are obtained at  $40 \times 10^6$  TM MCS.  $\bar{\phi} = 0.1$  is used here. (c) The free energy per chain at  $\chi = 0$  and 1.5 for the multi-chain systems with  $n = 2$  and 16, where the curves are shifted by  $C_0$  such that their value is 0 at  $4 \times 10^7$  TM MCS.  $L = N = 40$  and  $\bar{\phi} = 0.1$  is used here.

**Figure 3.** (a) Polymer segmental density profiles  $\phi(x)$  obtained from canonical-ensemble simulations on the 1D lattice with various  $n$  and the corresponding LSCF predictions at (a)  $\chi = 1$ . Part (b) shows how the difference in  $\phi(x)$  between FLMC and LSCF results,  $\epsilon_\phi$ , varies with  $n$ , where “ $k = -1$ ” denotes a straight line of slope  $-1$ .  $L = N = 40$  and  $\bar{\phi} = 0.1$  is used here.

**Figure 4.** (a) the brush height obtained from LSCF theory,  $h_{\text{LSCF}}$  and (b) the difference between the brush height obtained from WL-TM simulations,  $h_{\text{FLMC}}$ , and  $h_{\text{LSCF}}$  as functions of  $\chi$ .  $L = N = 40$  and  $\bar{\phi} = 0.1$  is used here.

**Figure 5.** Free-end distributions  $\phi_{s=N}(x)$  obtained from canonical-ensemble simulations on the 1D lattice with various  $n$  and the corresponding LSCF predictions at (a)  $\chi = 0$  and (b)  $\chi = 1$ . (c) the difference in the mean-square chain end-to-end distance between FLMC and LSCF results,  $R_{e\text{FLMC}}^2 - R_{e\text{LSCF}}^2$ , varies with  $n$ , where “ $k = -1$ ” denotes a straight line of slope  $-1$ .  $L = N = 40$  and  $\bar{\phi} = 0.1$  is used here.

**Figure 6.** (a) The LSCF predictions of the energy level  $E_{\text{LSCF}}/\rho_0^2$  and the internal energy per chain  $\beta u_{c,\text{LSCF}}$  as a function of  $\chi$ . (b) The difference in the ensemble-averaged energy level  $\langle E \rangle / \rho_0^2$  between WL-TM and LSCF results. (c) Fluctuations of local segmental densities around their average in canonical-ensemble simulations,  $\Delta\phi_1$ , where

“ $k = -1$ ” denotes a straight line of slope  $-1$  obtained from the unweighed least-squares fit using the data points at  $\chi = 0$  with  $n = 8$  and  $16$ . (d) The difference between the square of the ensemble-averaged density profile in canonical-ensemble simulations and the corresponding LSCF prediction,  $\Delta\phi_2$ , where “ $k = -1$ ” denotes a straight line of slope  $-1$ . (e) The difference in the internal energy per chain between WL-TM and LSCF results,  $\beta(u_{c,\text{FLMC}} - u_{c,\text{LSCF}})$ .  $L = N = 40$  and  $\bar{\phi} = 0.1$  is used here.

**Figure 7.** (a) WL-TM simulations of the fluctuations of energy level  $(\langle E^2 \rangle - \langle E \rangle^2) / \rho_0^4$  as a function of  $\chi$  for different  $n$ , both its LSCF prediction is 0. (b) The canonical-ensemble averaged  $(\langle E^2 \rangle - \langle E \rangle^2) / \rho_0^4$  as a function of  $n$ , where “ $k = -1$ ” denotes a straight line of slope  $-1$ .  $L = N = 40$  and  $\bar{\phi} = 0.1$  is used here.

**Figure 8.** (a) LSCF predictions of the difference in free energy per chain,  $\beta\Delta f_c$ , and that in entropy per chain,  $\Delta s_c/k_B$ , from the ideal reference state in the limit of  $\chi \rightarrow -\infty$ . (b) The difference in free energy per chain between WL-TM and LSCF results,  $\beta(\Delta f_{c,\text{FLMC}} - \Delta f_{c,\text{LSCF}})$ , as a function of  $\chi$ . (c)  $\beta(\Delta f_{c,\text{FLMC}} - \Delta f_{c,\text{LSCF}})$  as a function of  $n$ , where “ $k = -1$ ” denotes a straight line of slope  $-1$  obtained from the unweighed least-squares fit using the data points at  $\chi = 0$ . (d) The difference in entropy per chain between WL-TM and LSCF results,  $(\Delta s_{c,\text{FLMC}} - \Delta s_{c,\text{LSCF}})/k_B$  as a function of  $\chi$ . (e)  $(\Delta s_{c,\text{FLMC}} - \Delta s_{c,\text{LSCF}})/k_B$  as a function of  $n$ .

**Figure 9.** The difference in polymer segmental density profile between brushes in an implicit and an explicit solvent,  $\Delta\phi$ , as a function of  $\bar{\phi}$  for  $N = 40$  obtained from LSCF calculations; see text for details.

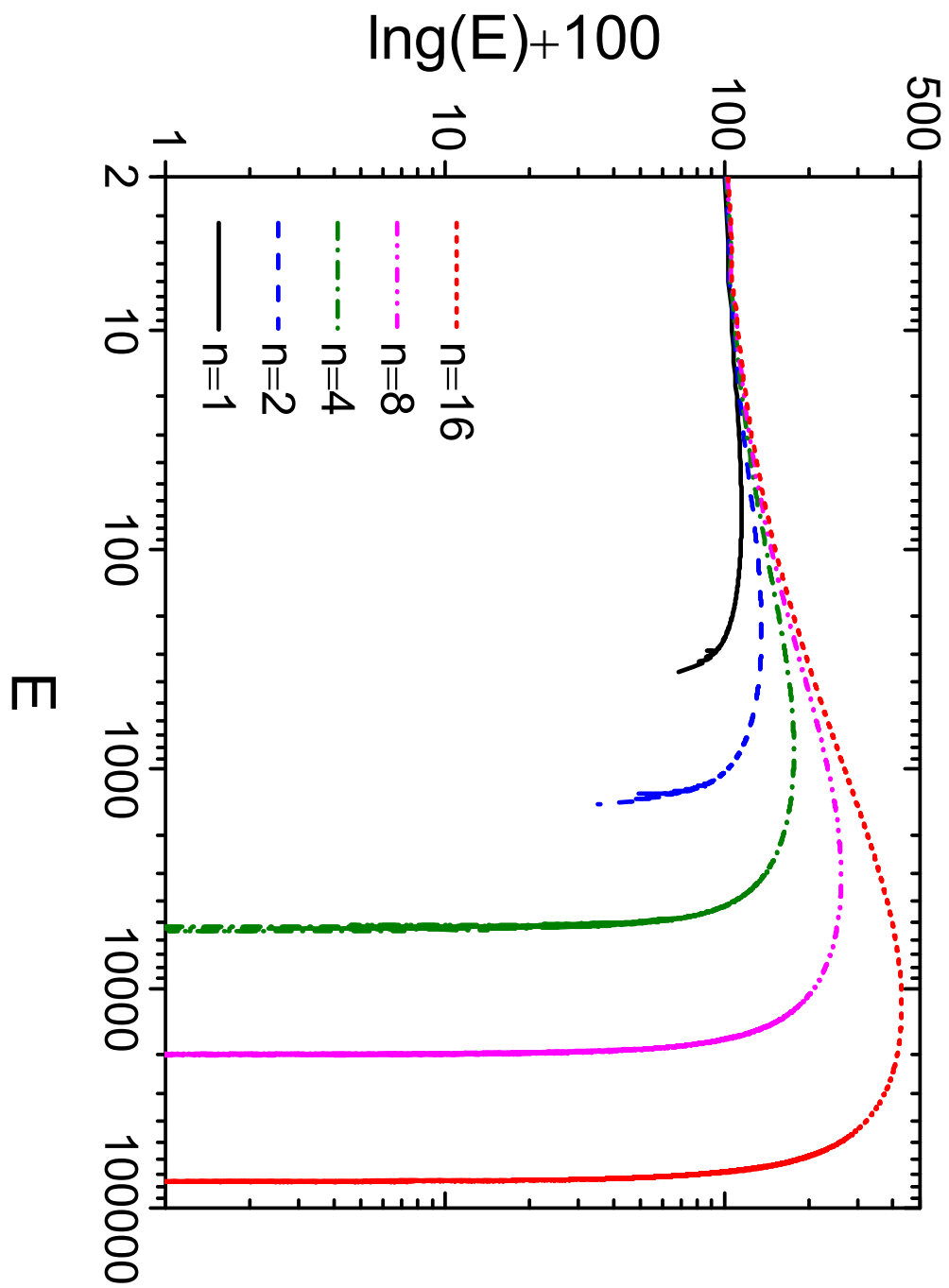


Figure 1: (a)

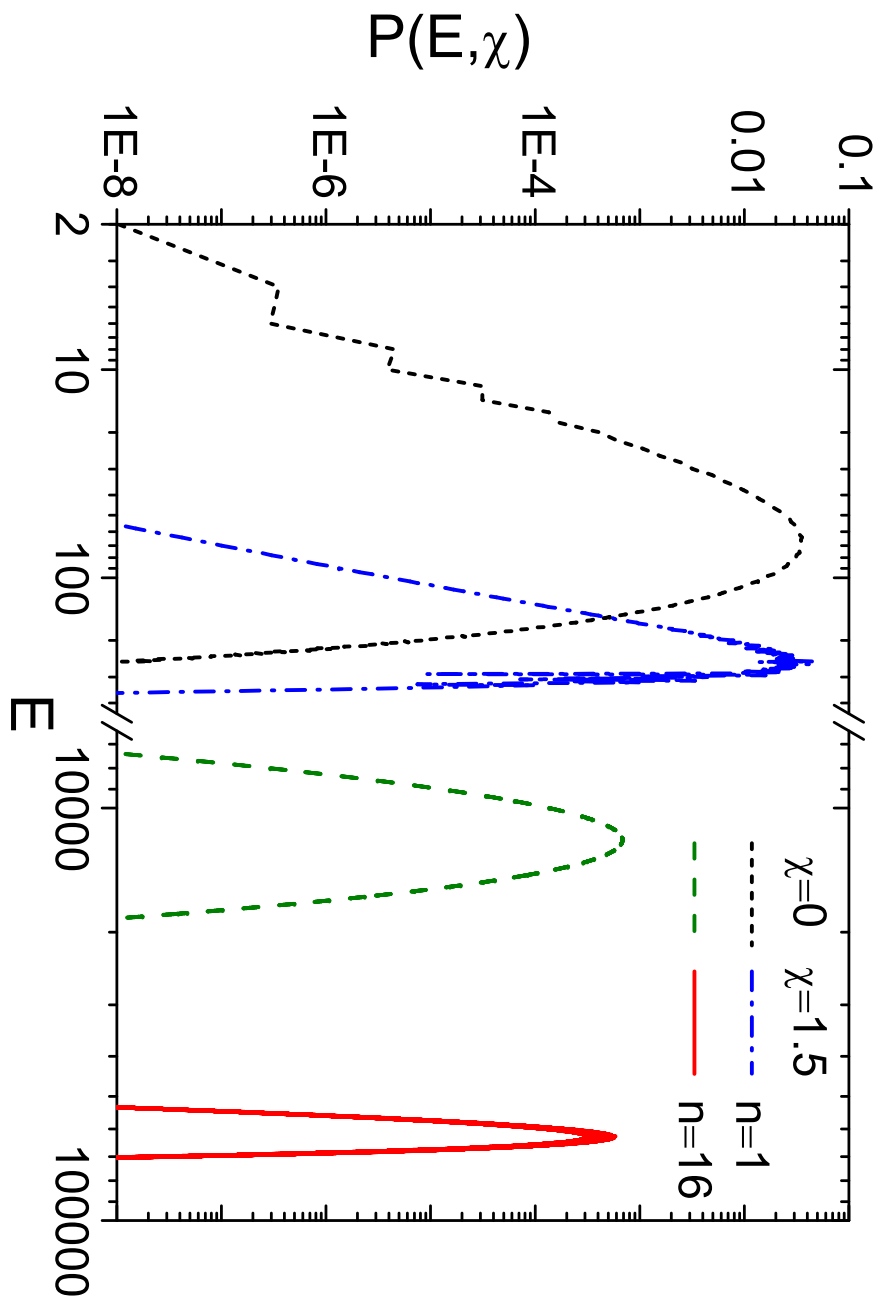


Figure 1: (b)

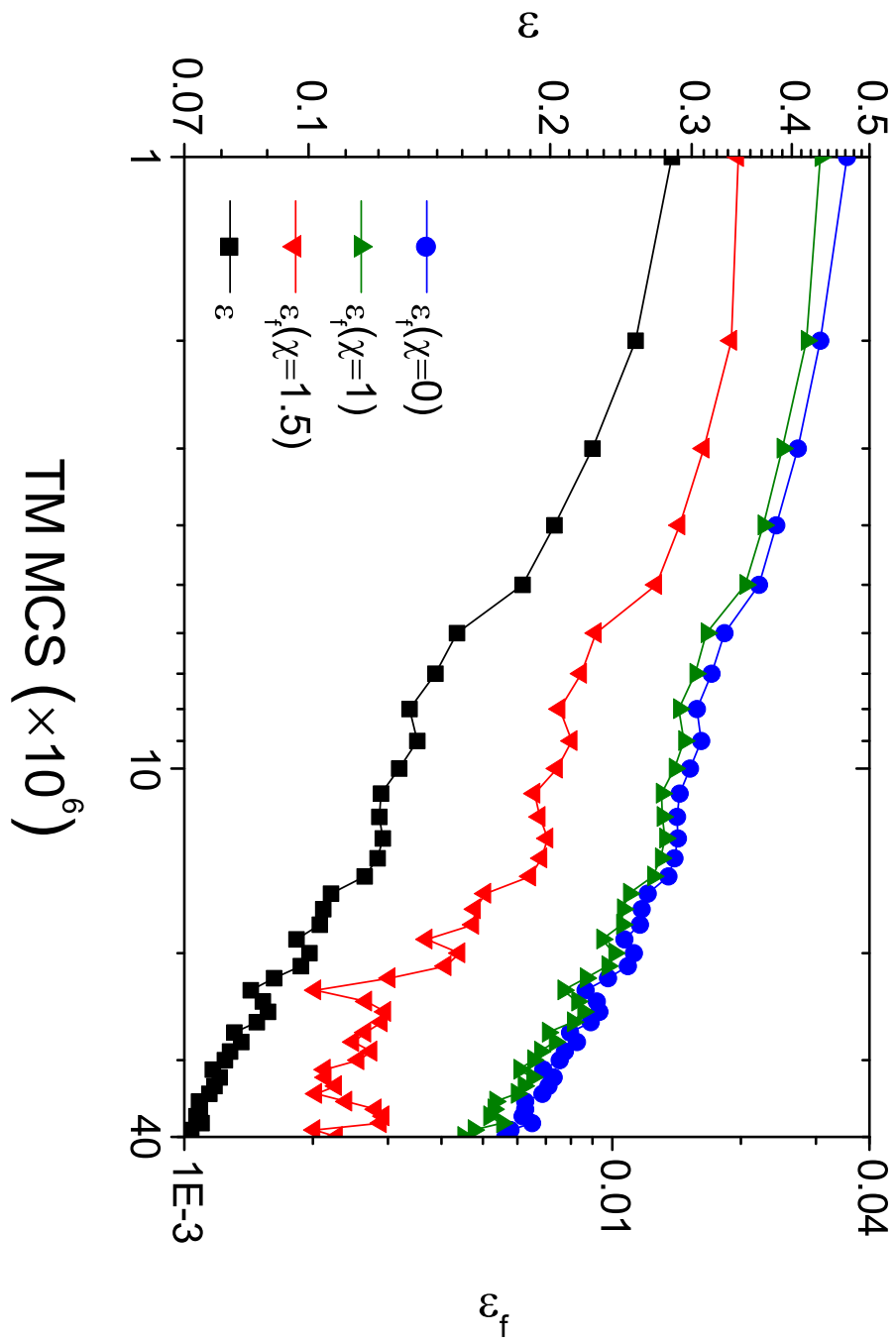


Figure 2: (a)

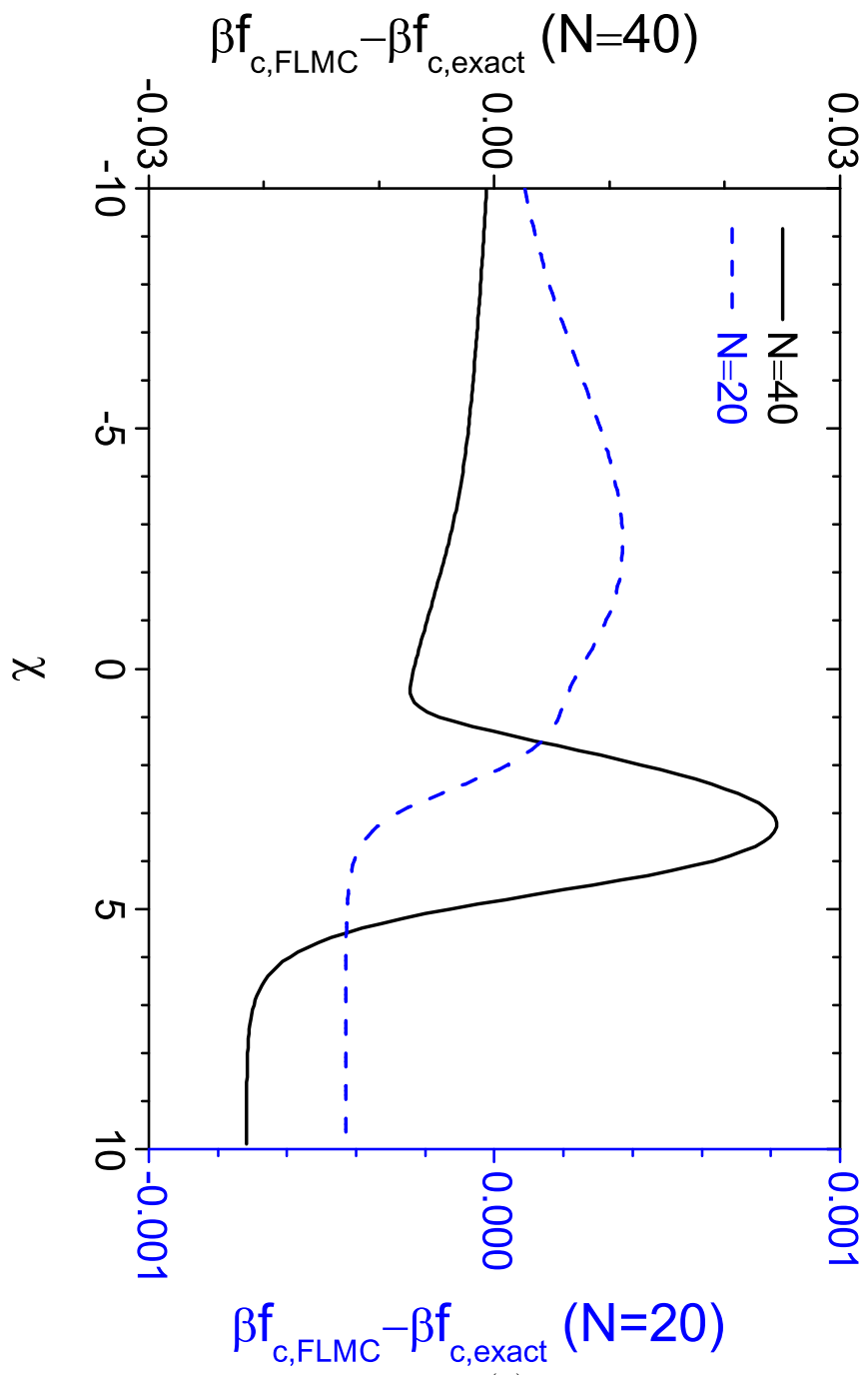


Figure 2: (b)

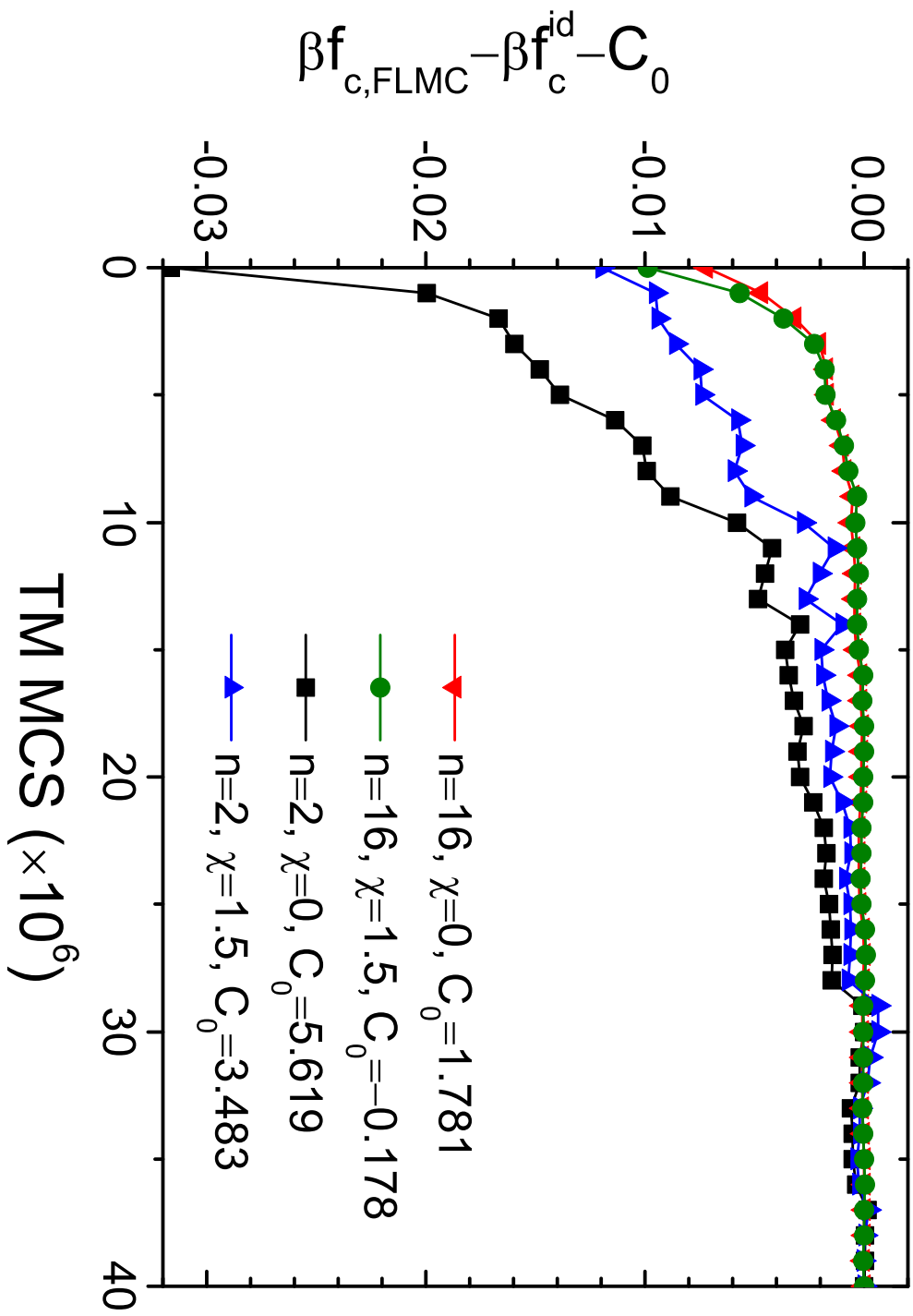


Figure 2: (c)

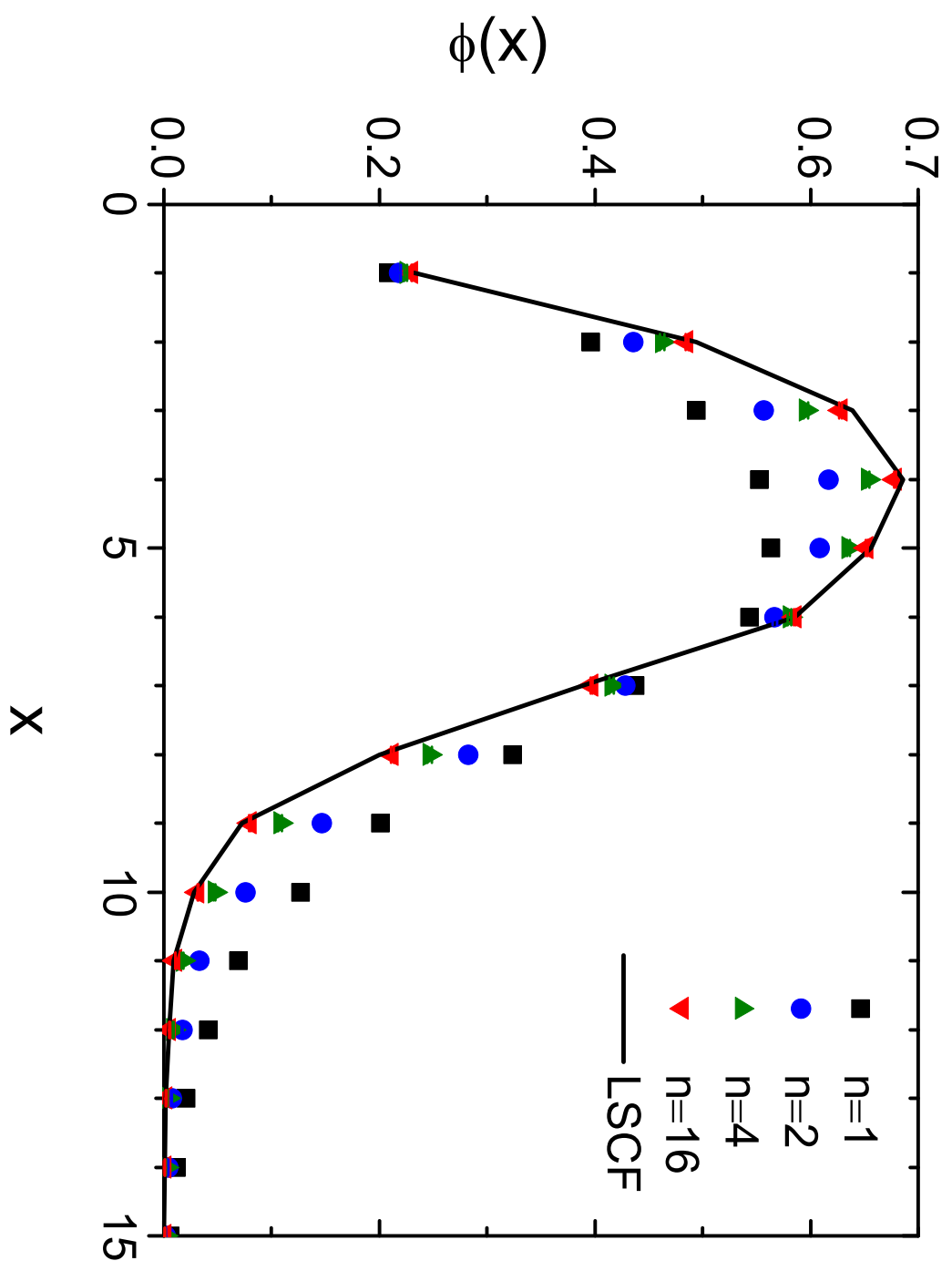


Figure 3: (a)

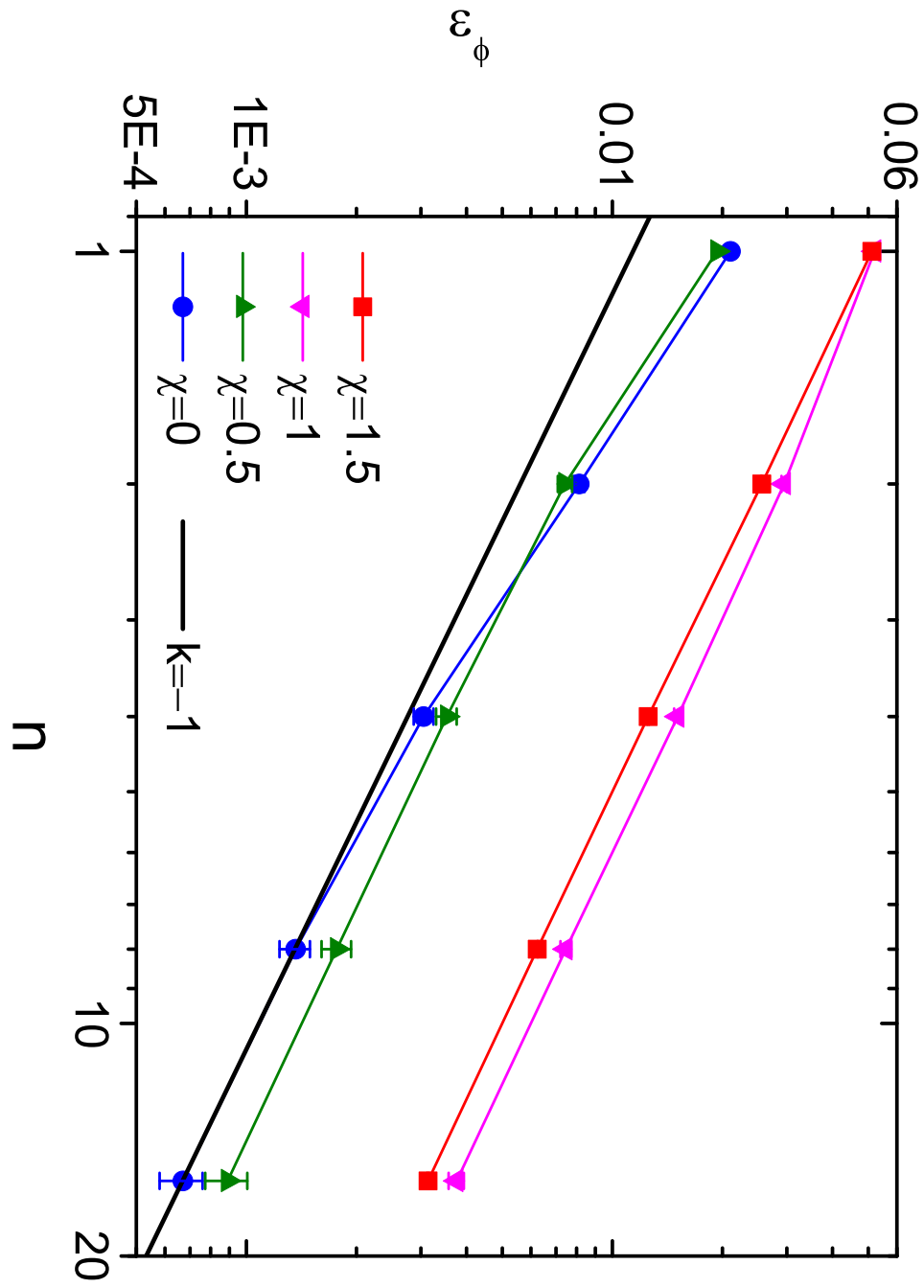


Figure 3: (b)

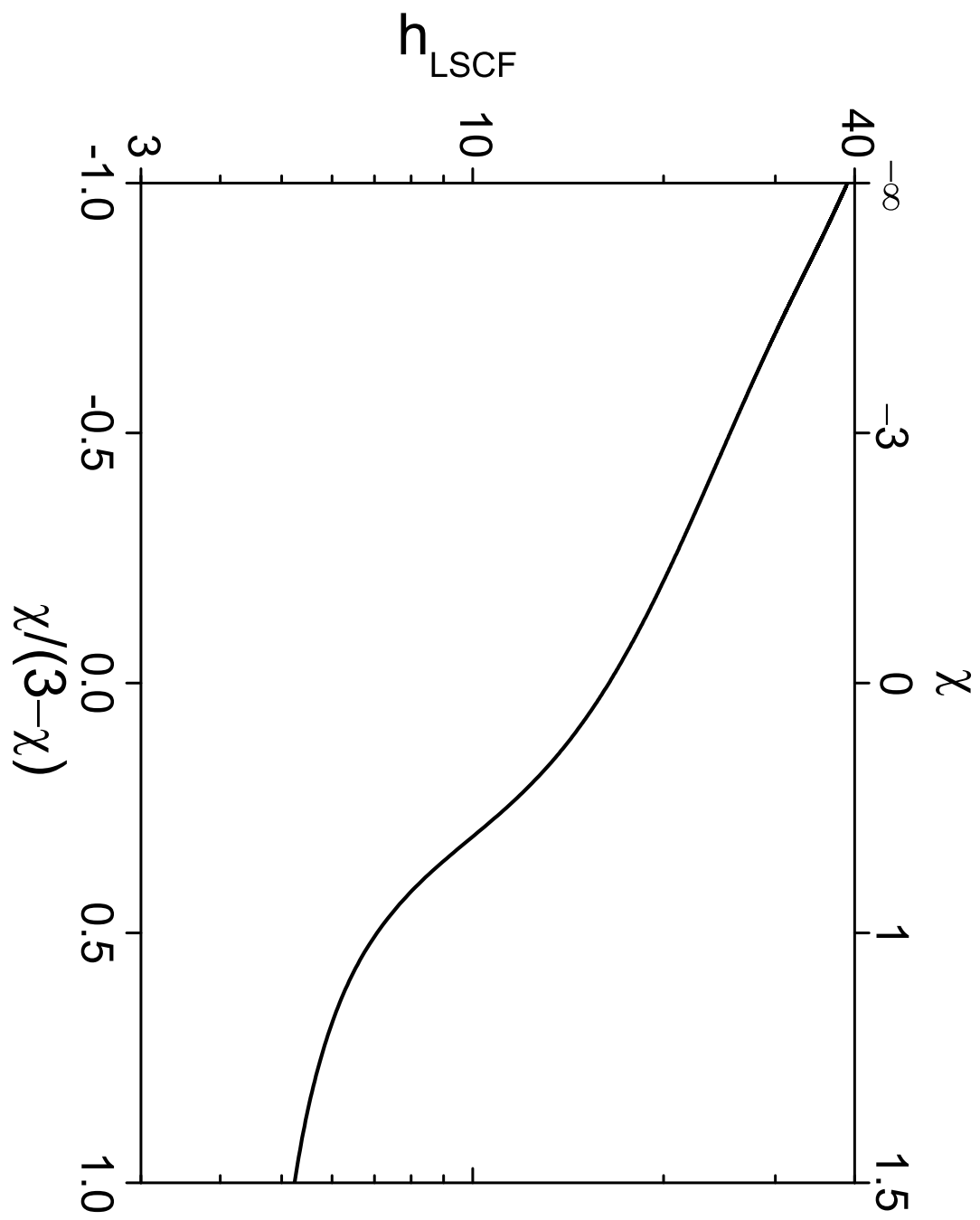


Figure 4: (a)

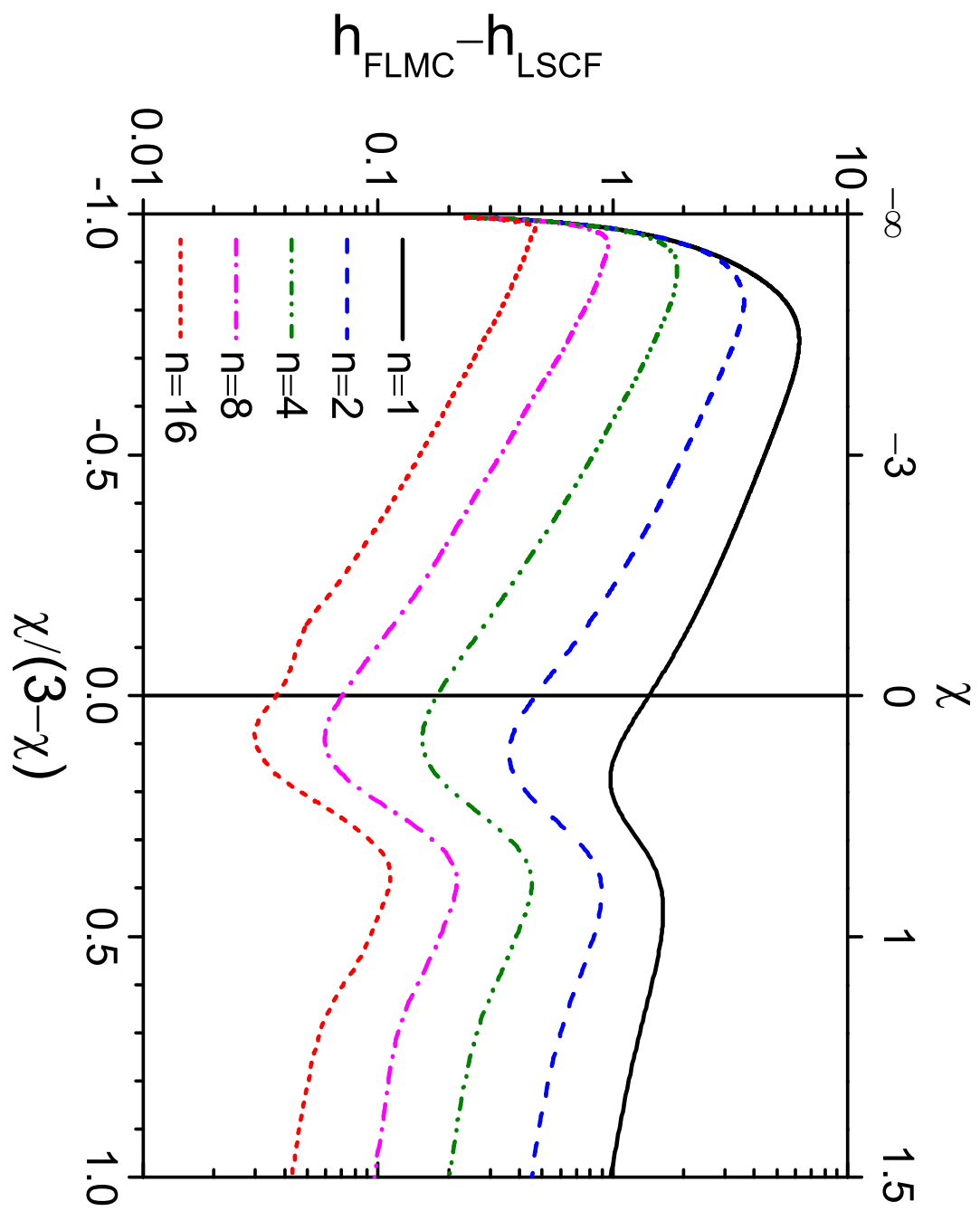


Figure 4: (b)

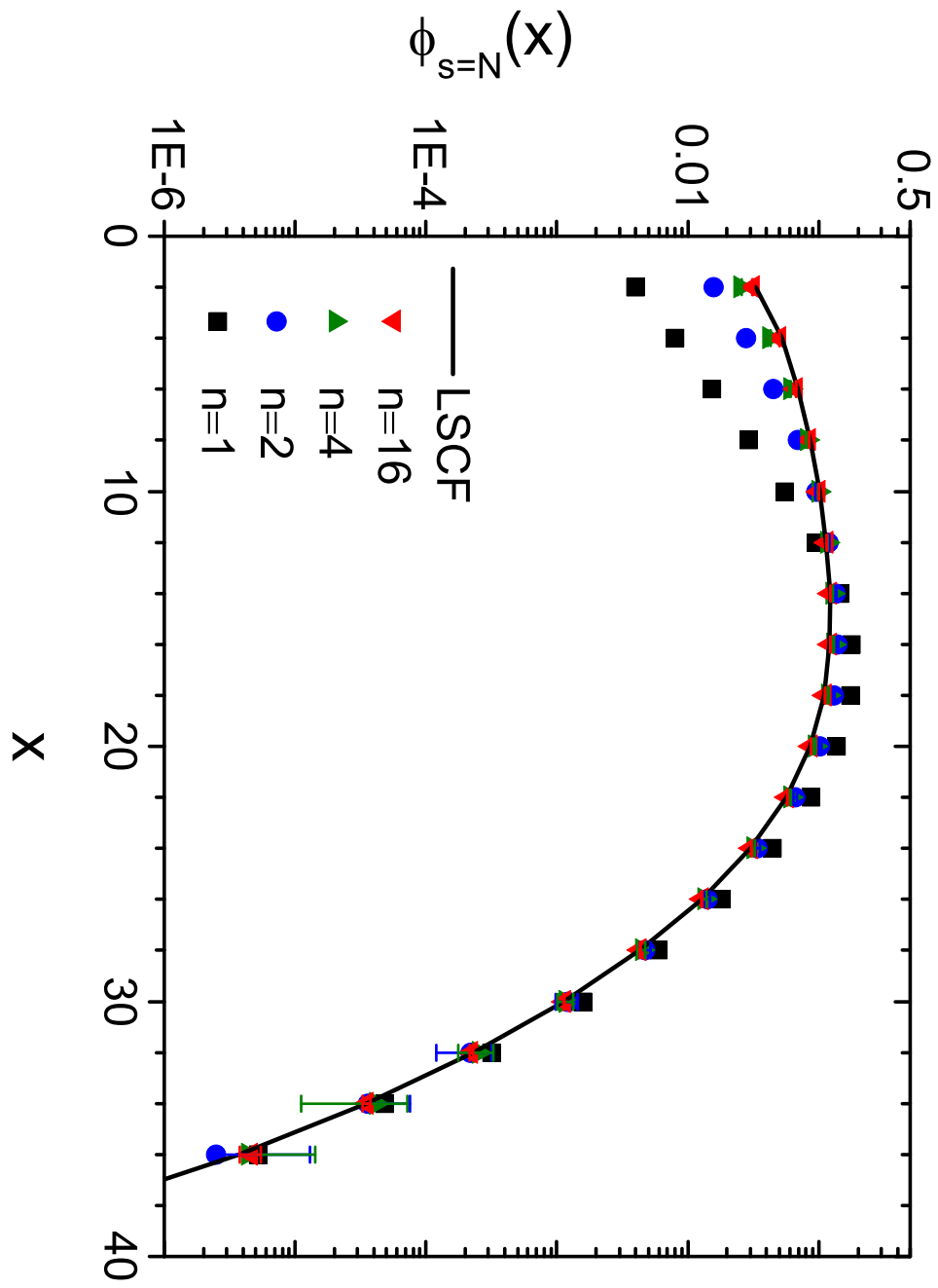


Figure 5: (a)

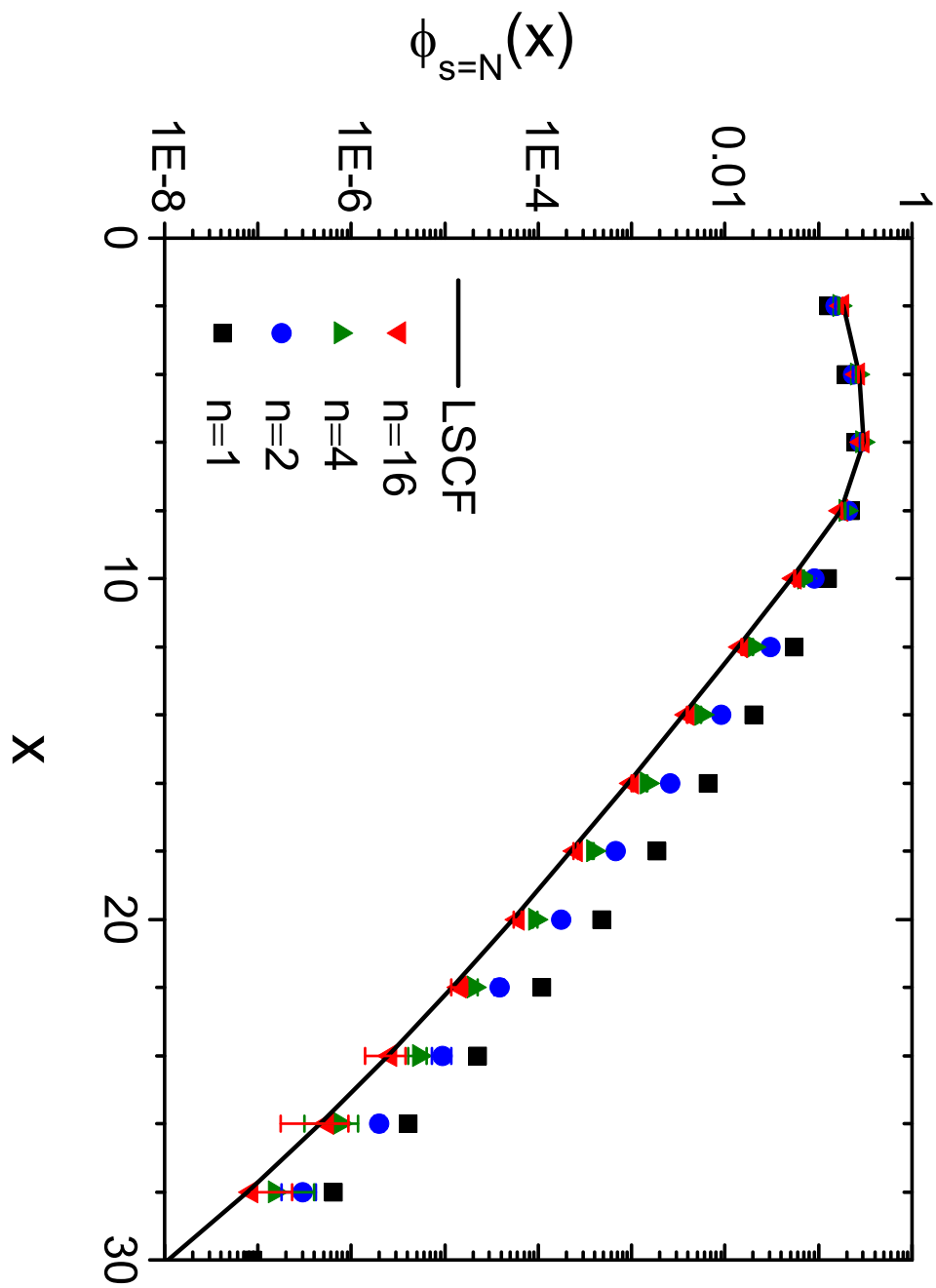


Figure 5: (b)

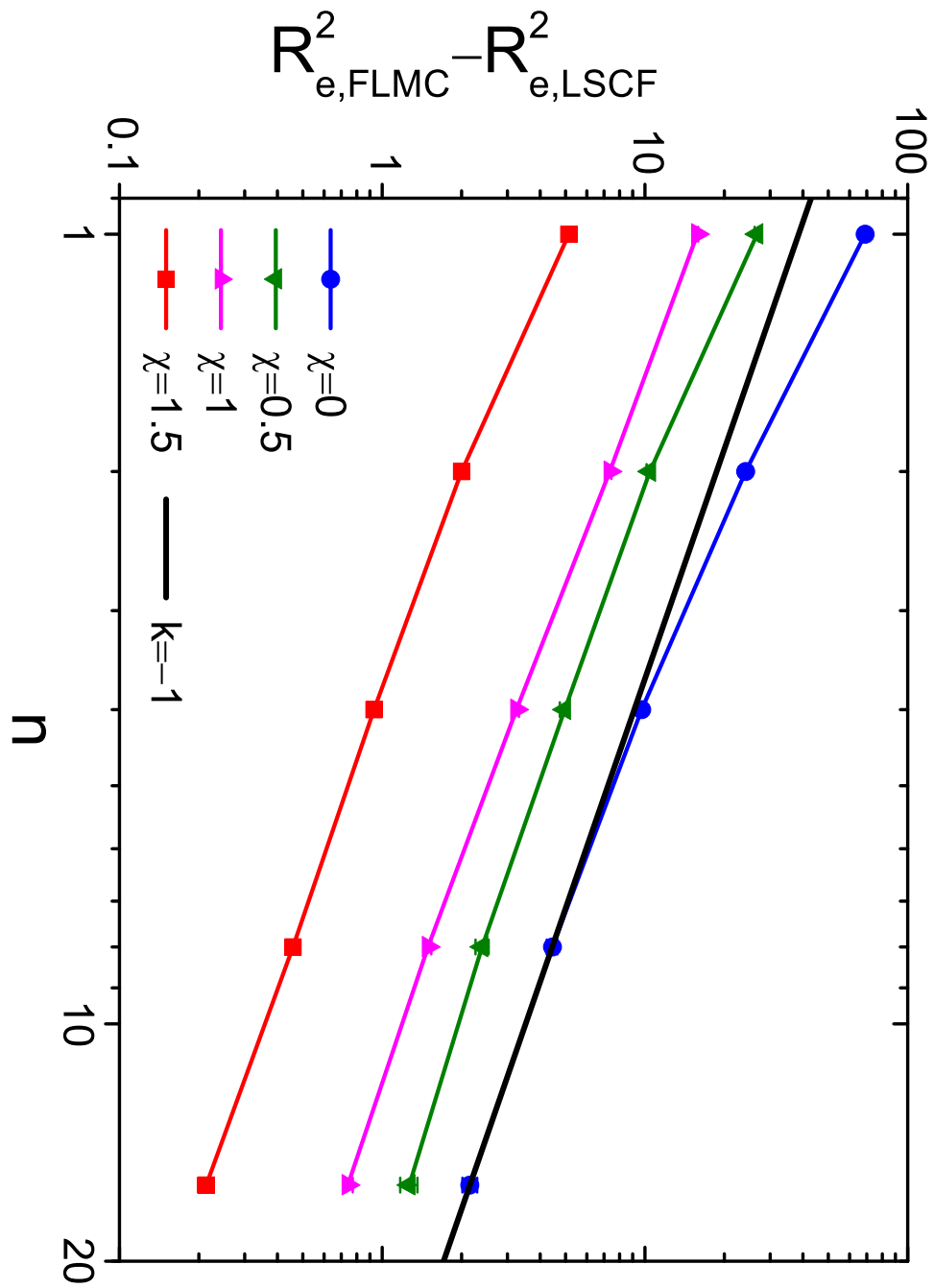


Figure 5: (c)

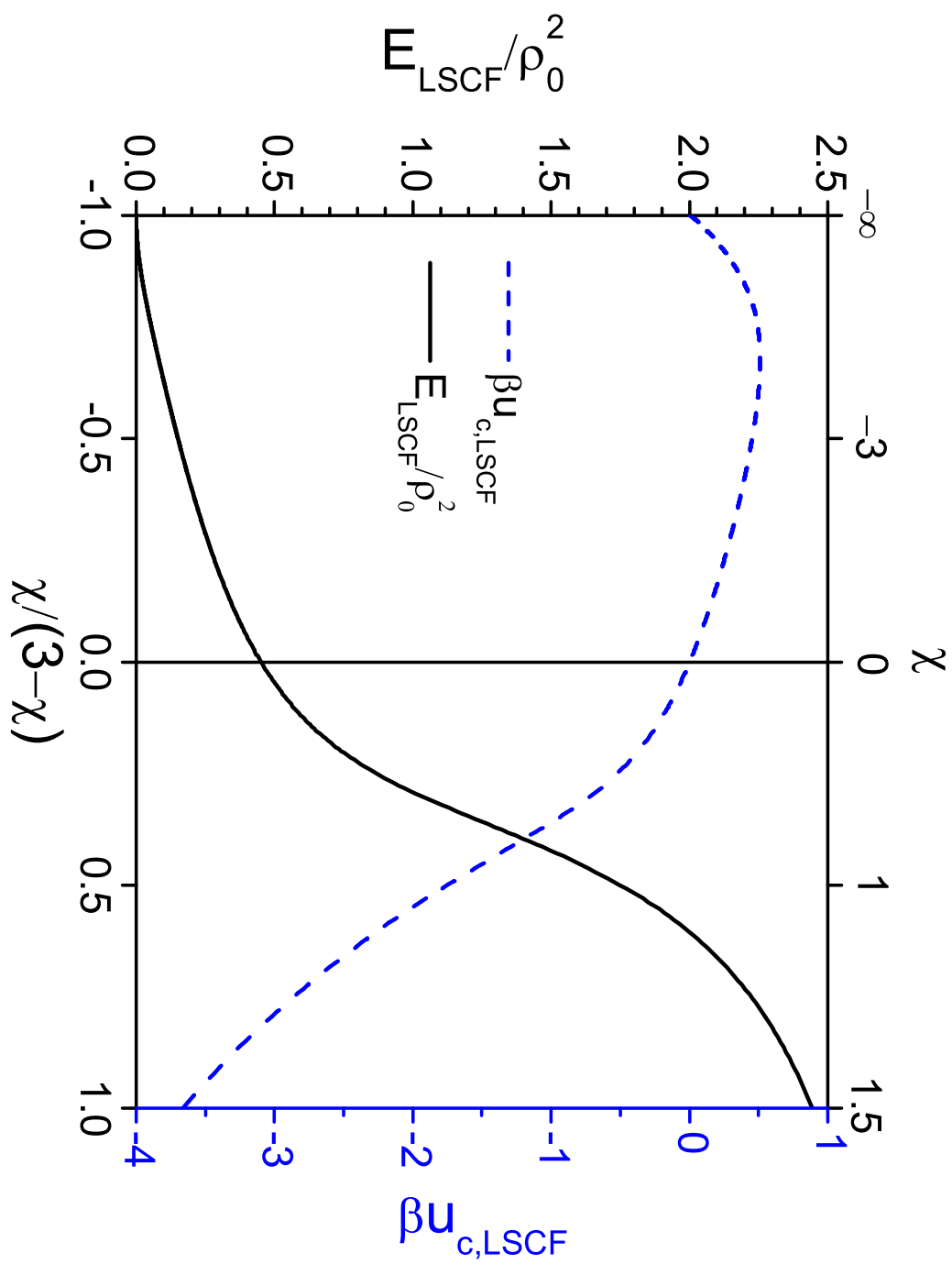


Figure 6: (a)

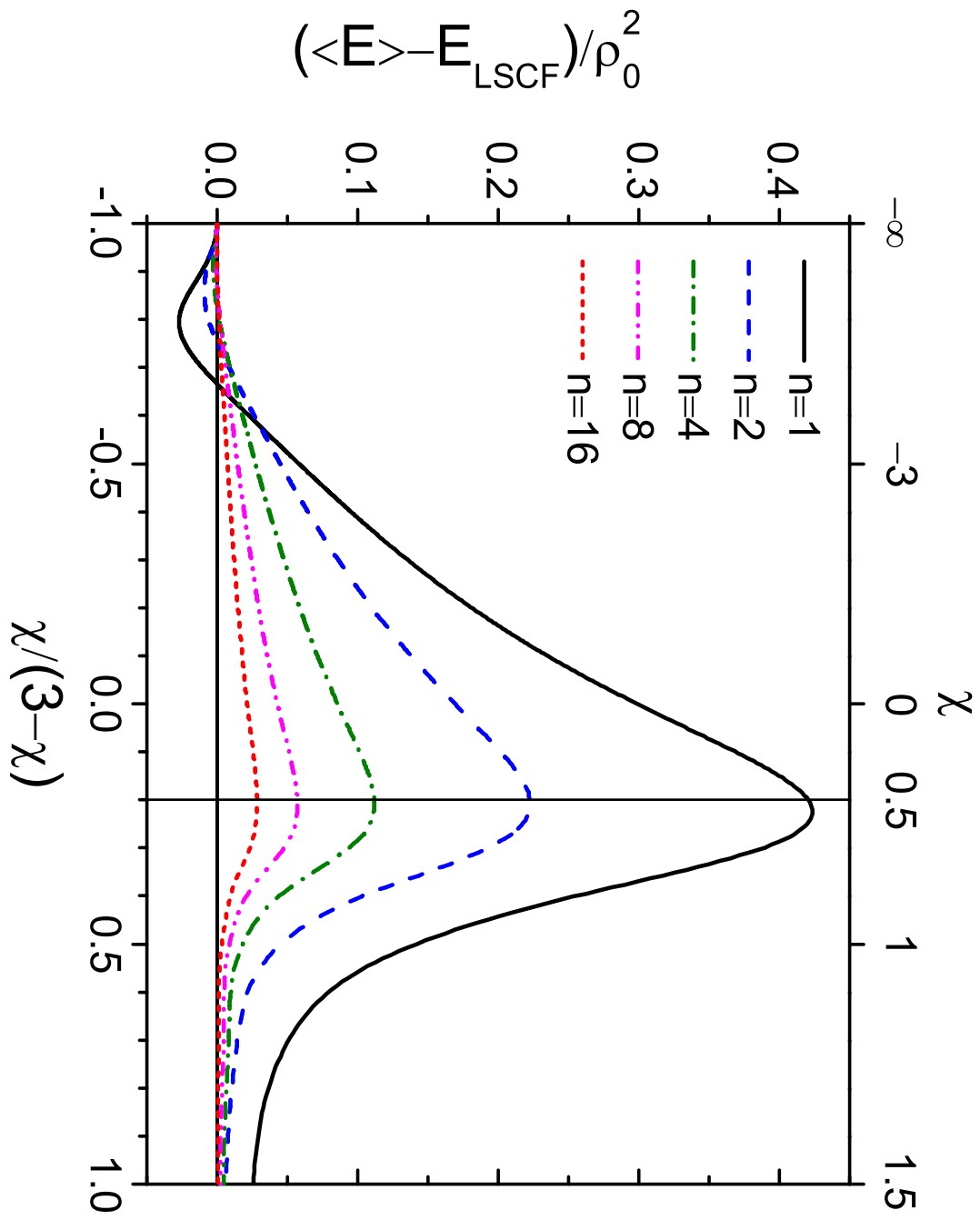


Figure 6: (b)

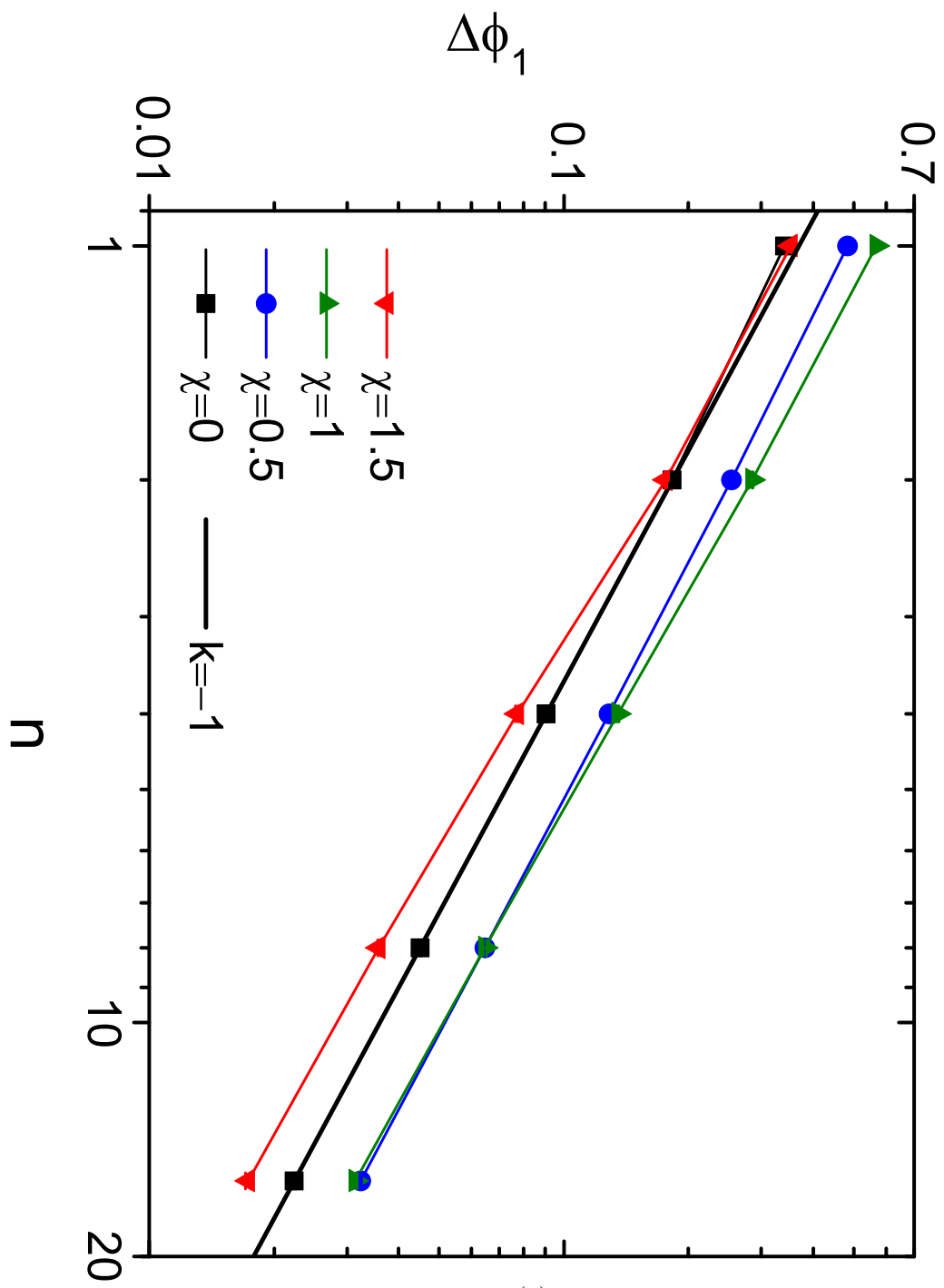


Figure 6: (c)

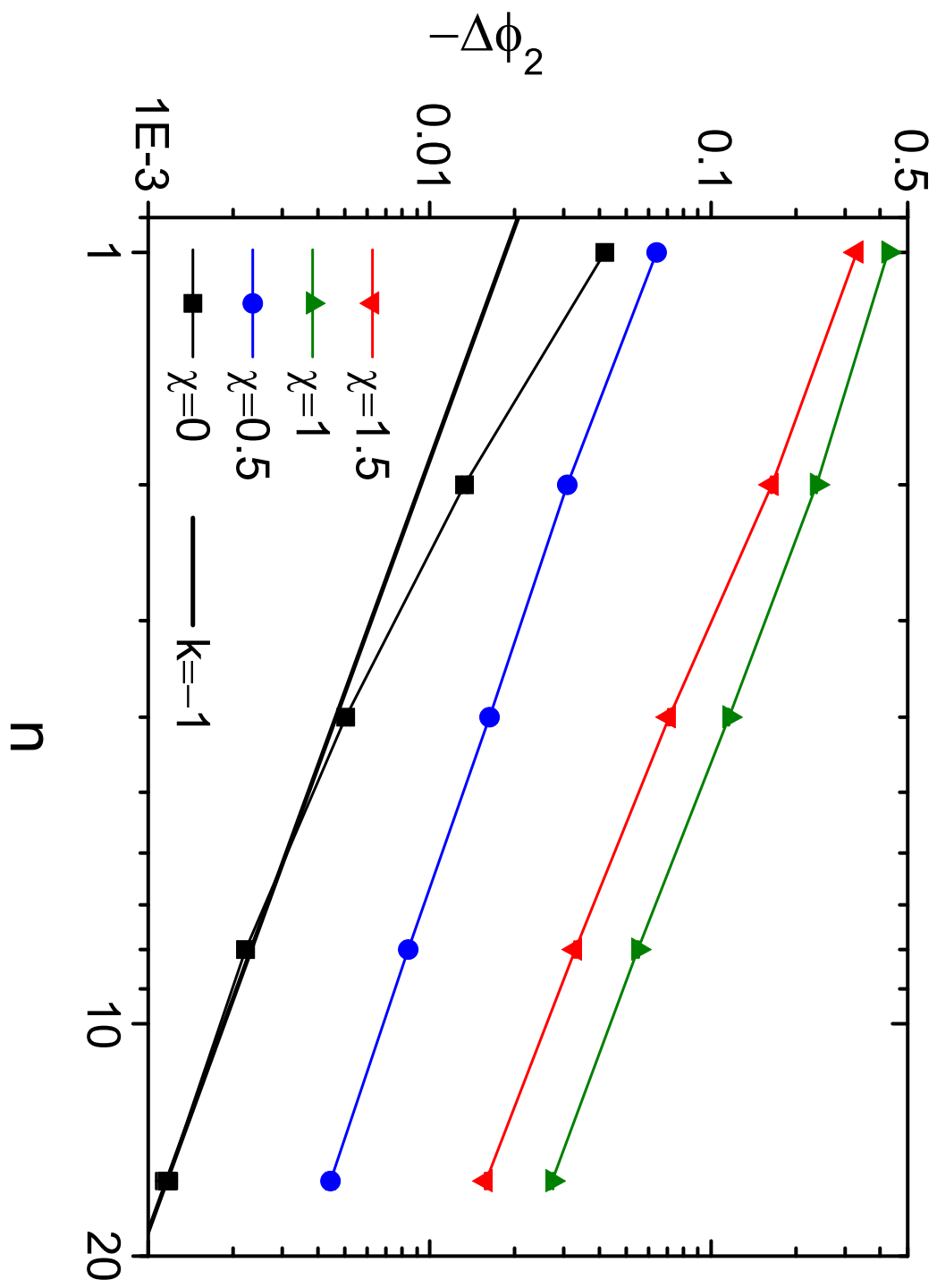


Figure 6: (d)

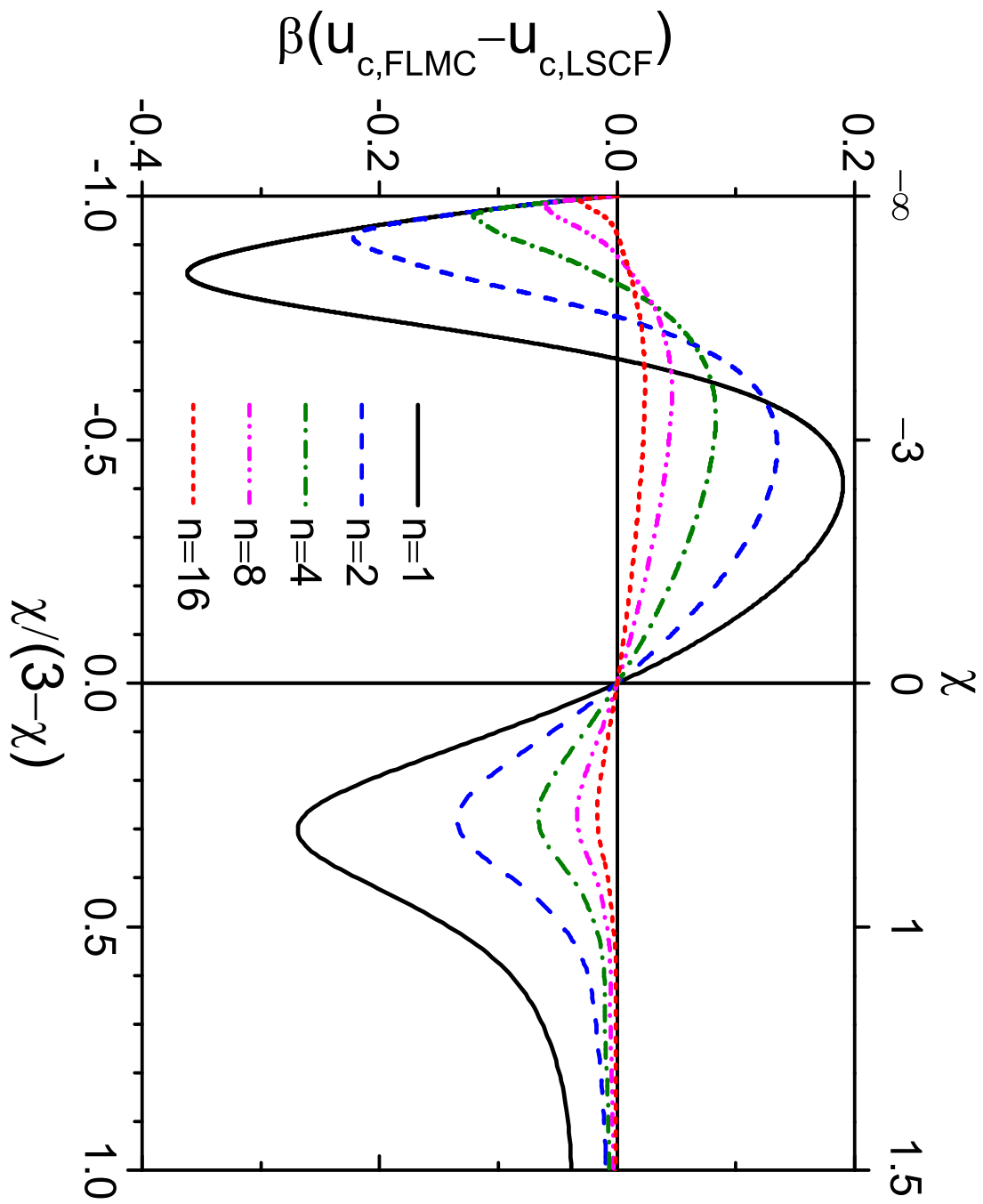


Figure 6: (e)

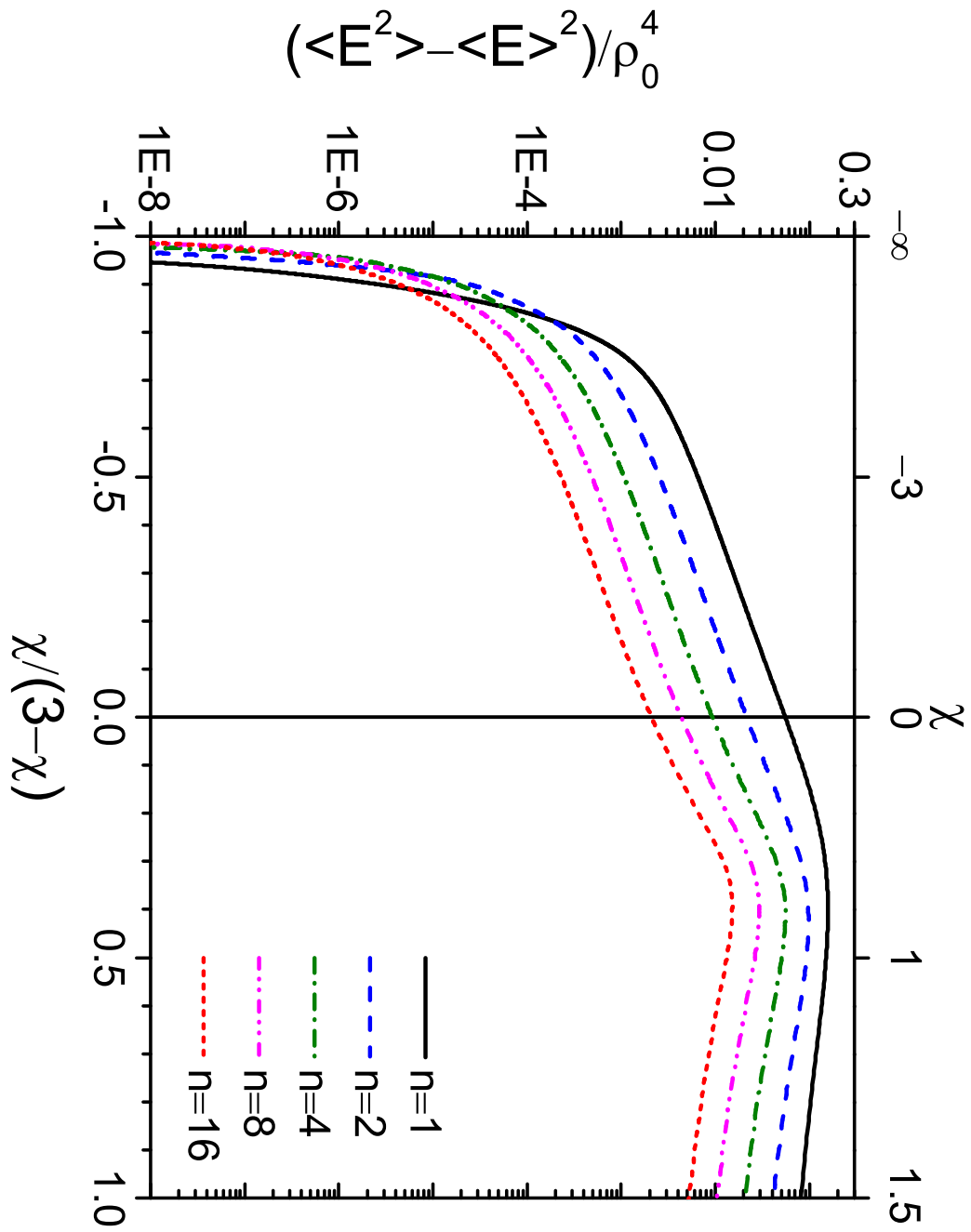


Figure 7: (a)

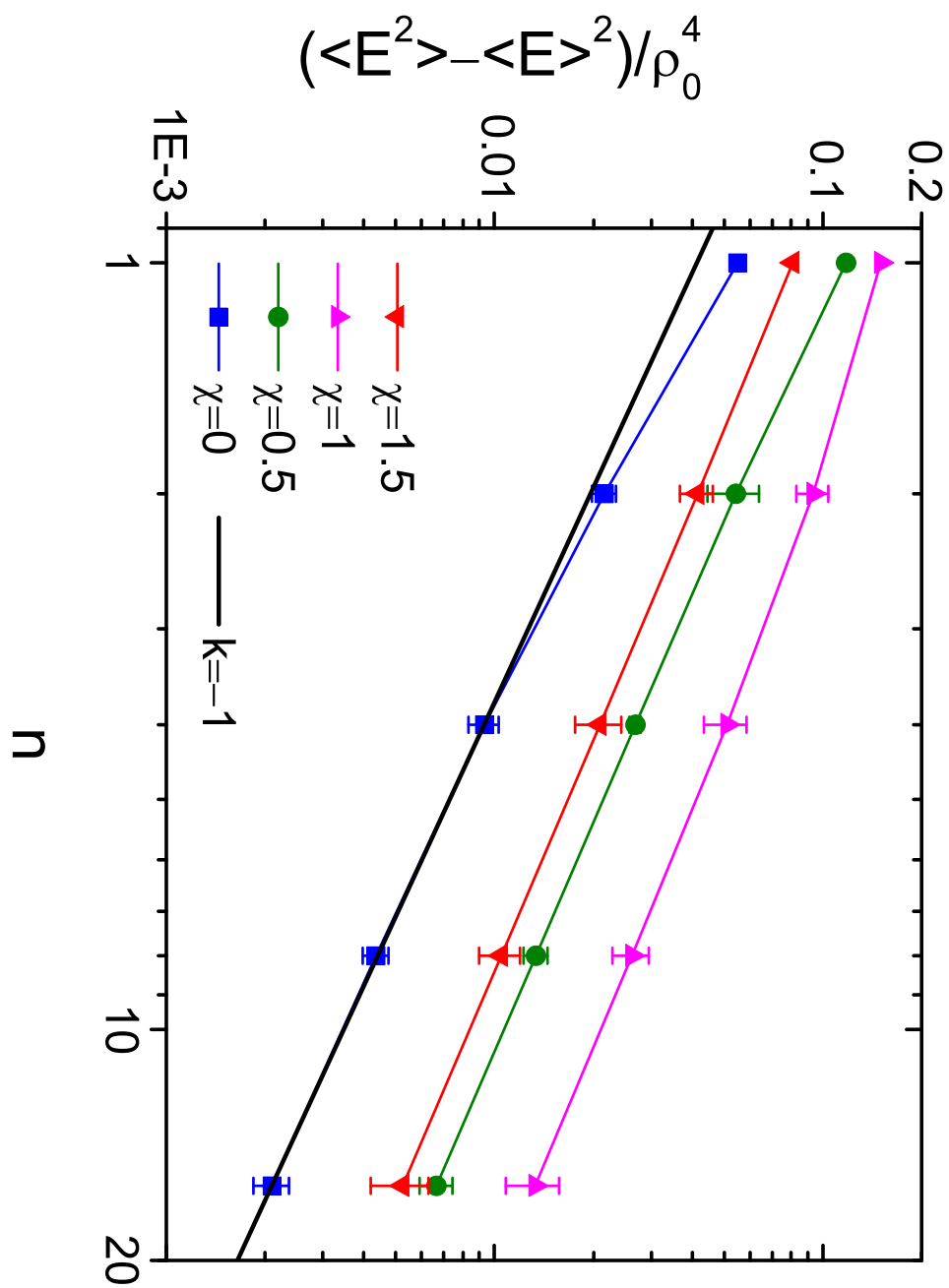


Figure 7: (b)

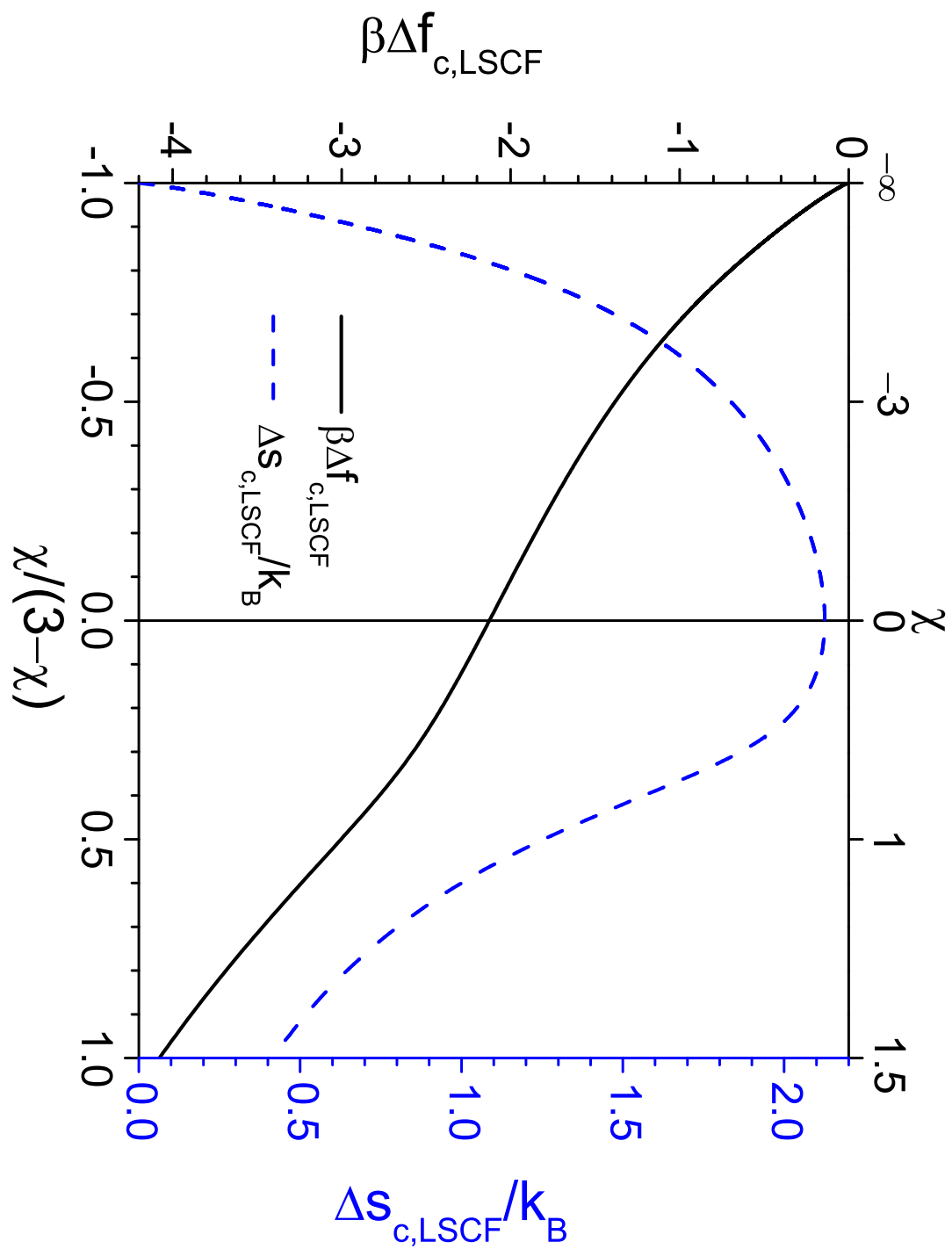


Figure 8: (a)

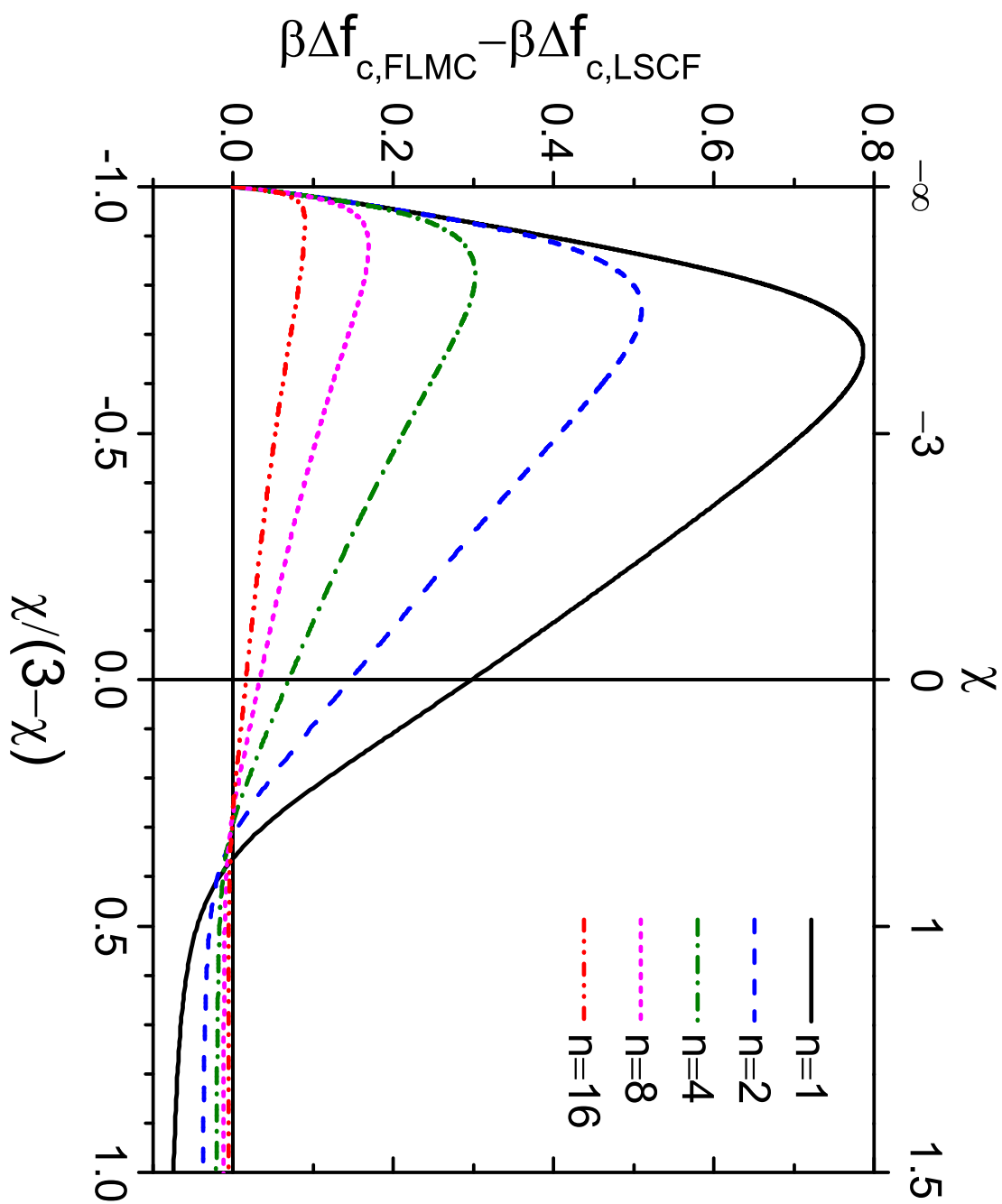


Figure 8: (b)

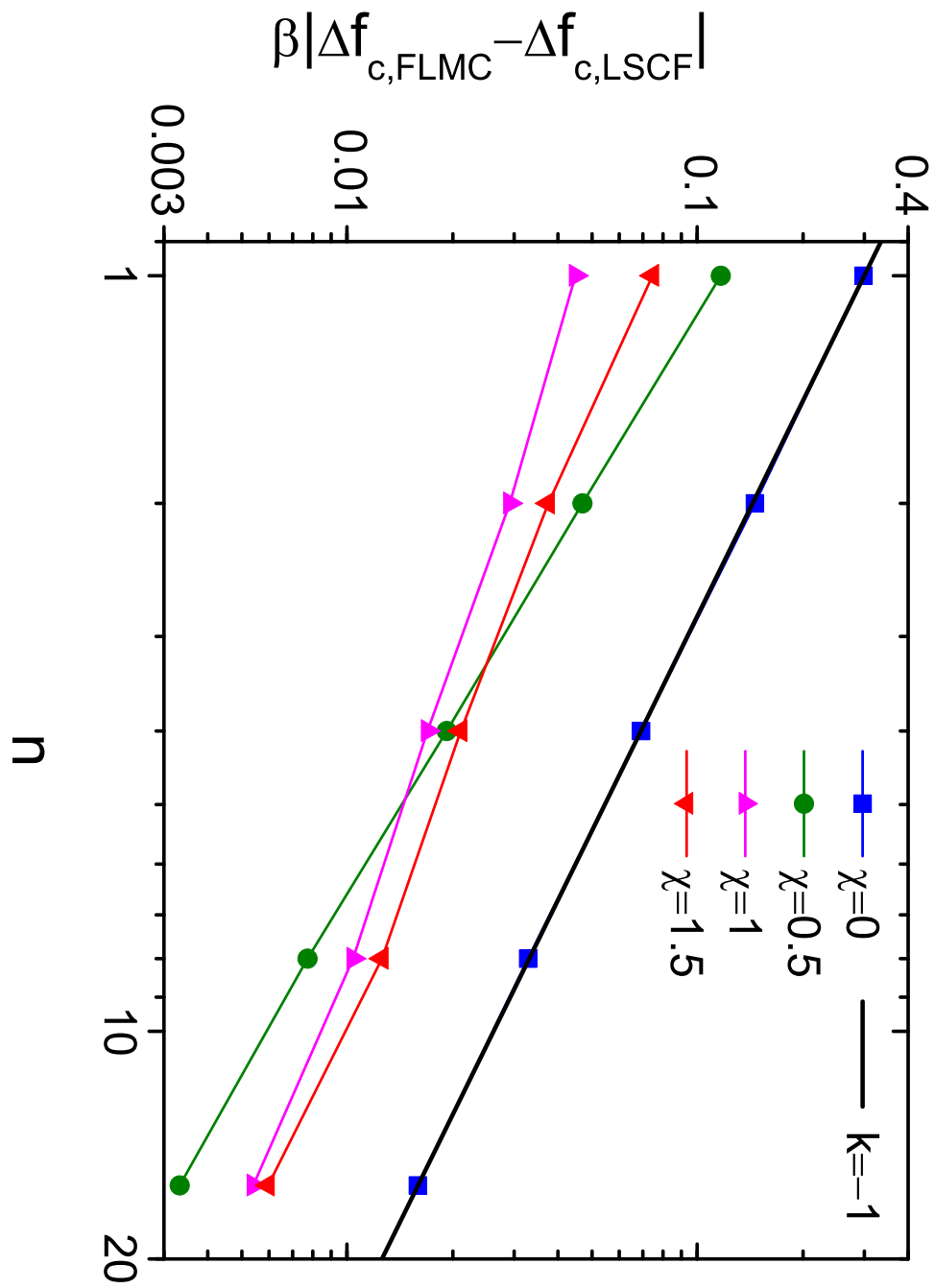


Figure 8: (c)

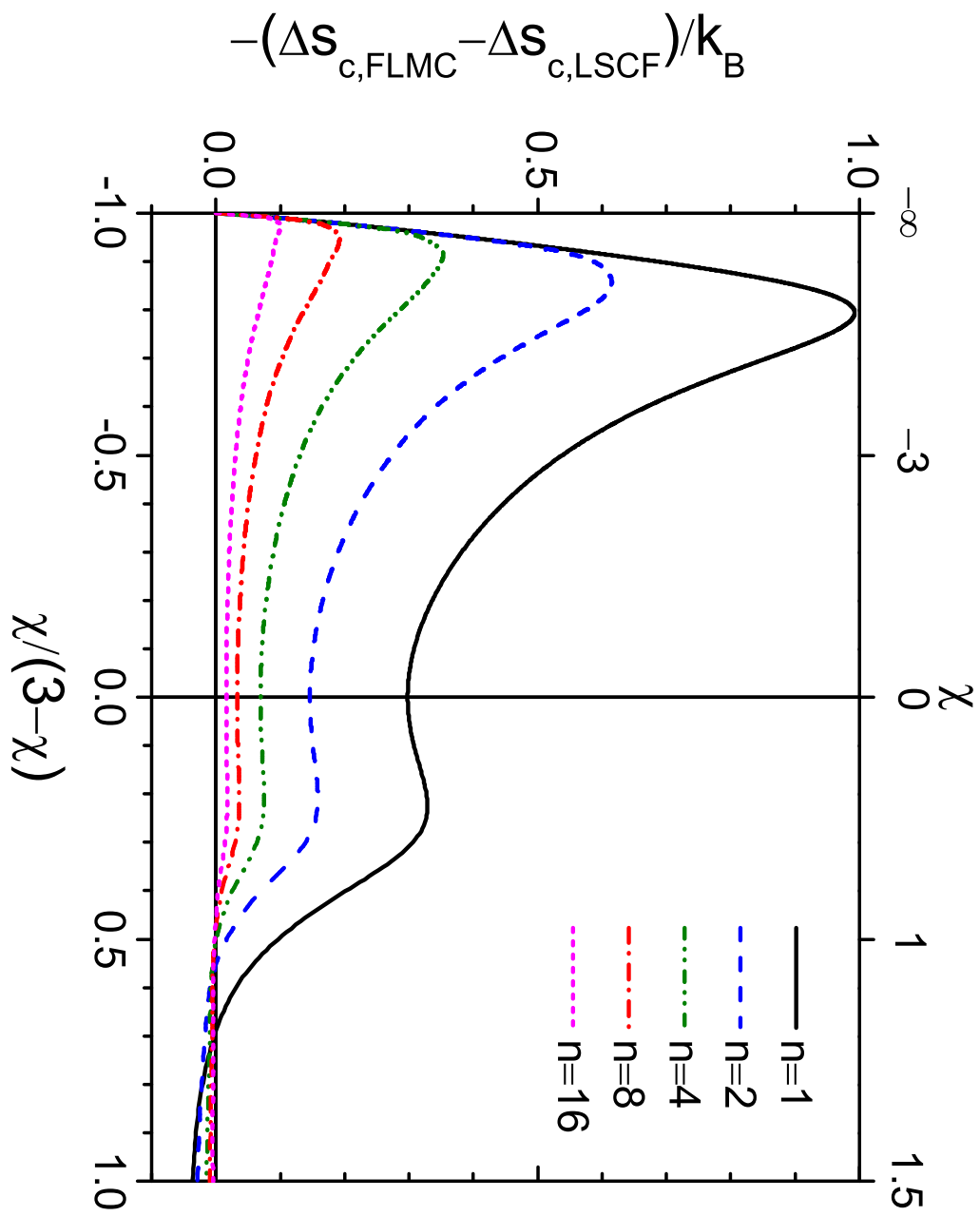


Figure 8: (d)

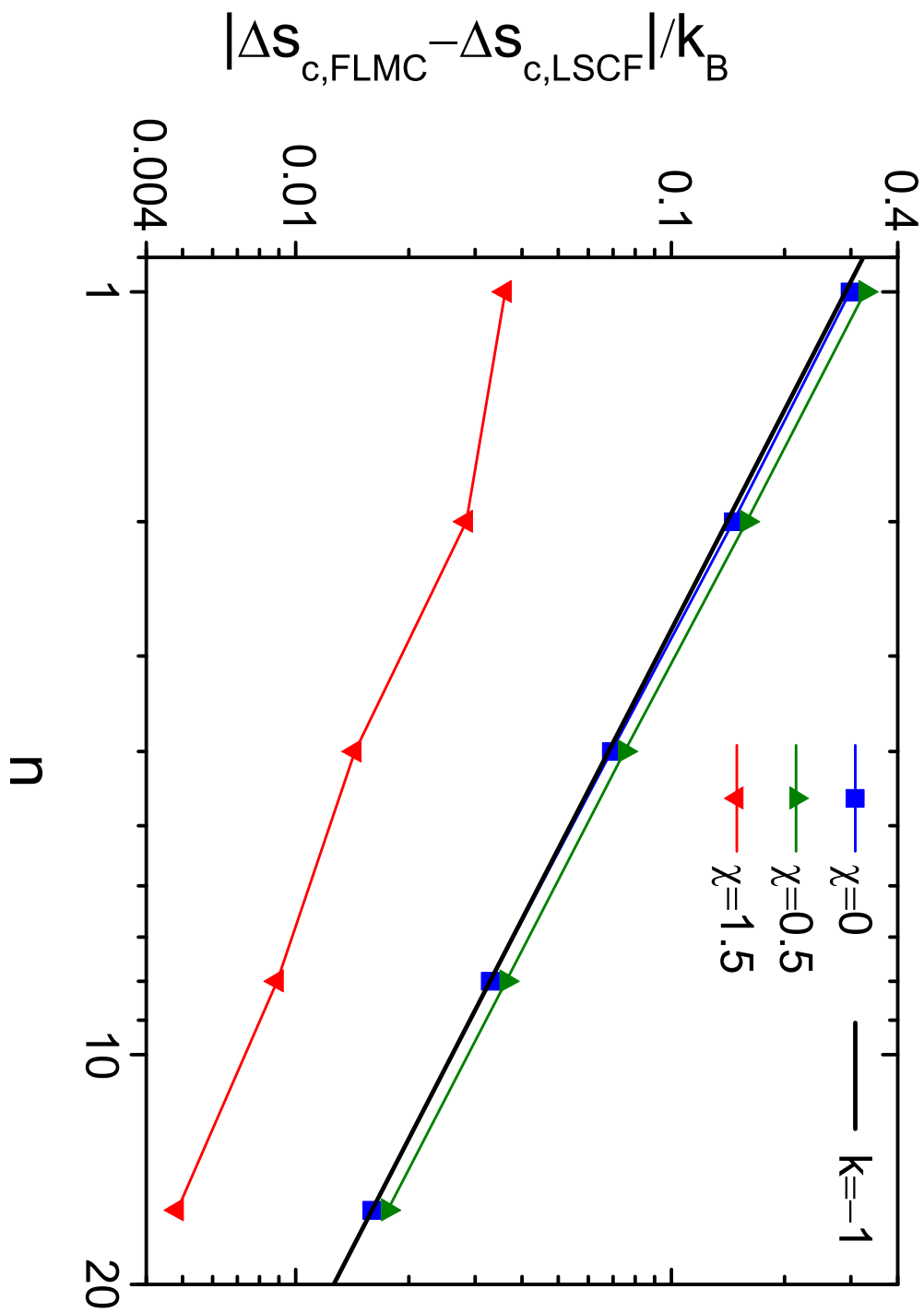


Figure 8: (e)

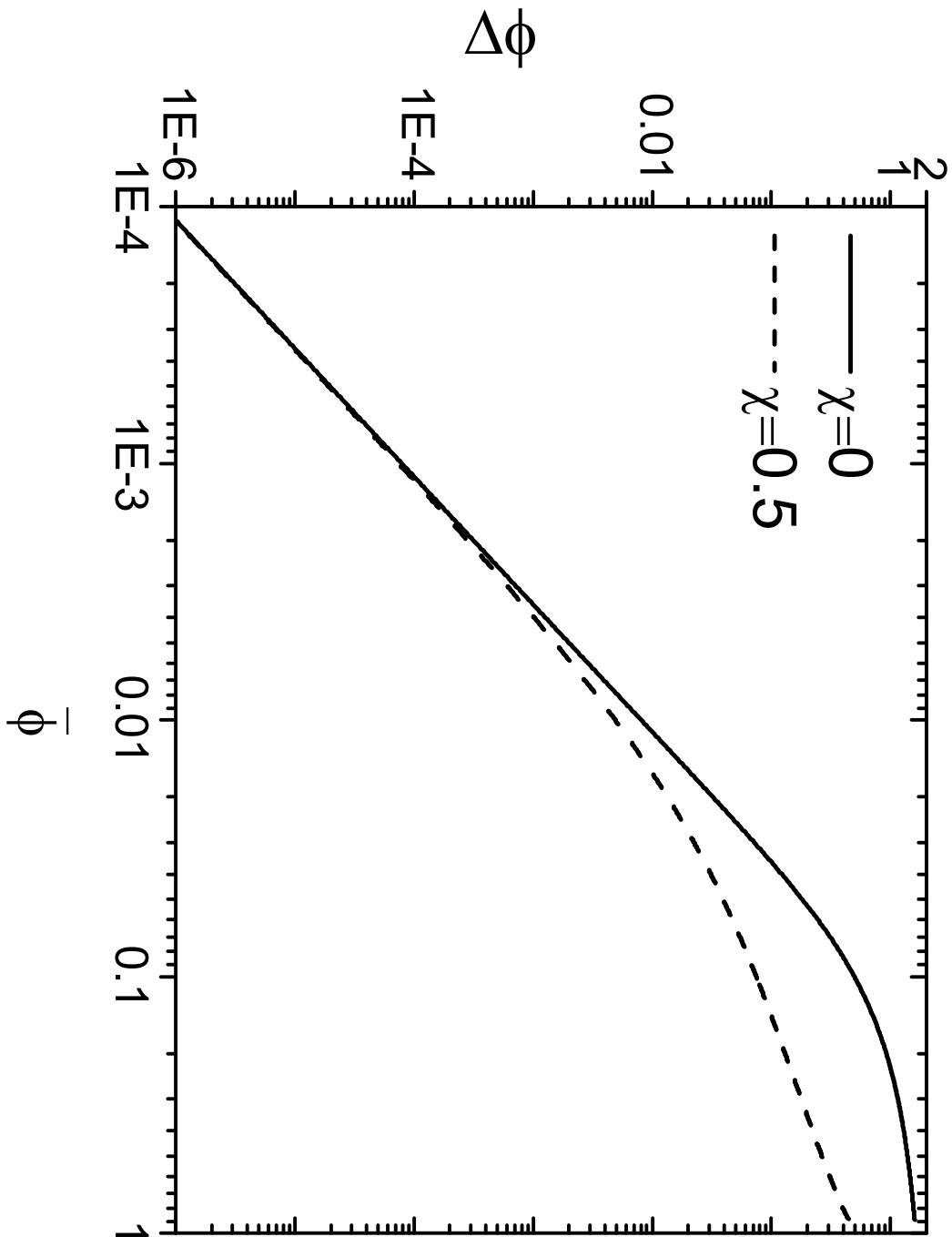
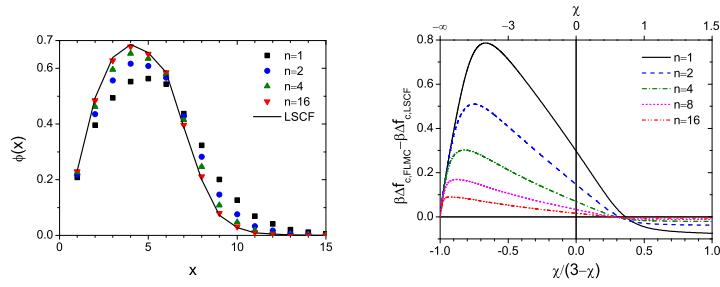


Figure 9:

for Table of Contents use only



**Title:** Quantitative Study of Fluctuation Effects by Fast Lattice Monte Carlo Simulations. III. Homopolymer Brushes in an Explicit Solvent

**Authors:** Pengfei Zhang<sup>1,2</sup>, Baohui Li<sup>1</sup>, and Qiang Wang<sup>2</sup>

<sup>1</sup>School of Physics, Nankai University, Tianjin, P. R. China 300071

<sup>2</sup>Department of Chemical and Biological Engineering, Colorado State University, Fort Collins, CO 80523-1370